

Evaluation of ground motion models for Northern Vietnam based on ground motion records of the 2020 Mw5.0 Moc-Chau earthquake sequence

Earthquake Spectra

1–32





© The Author(s) 2024

Article reuse guidelines:

sagepub.com/journals-permissions

DOI: 10.1177/87552930241285177

journals.sagepub.com/home/eqs

Van-Bang Phung^{1,8} , Bor-Shouh Huang¹, Cong Nghia Nguyen^{1,3} , Van Duong Nguyen^{3,4}, Le Minh Nguyen^{3,4}, Anh Duong Nguyen³, Quang Khoi Le³, The Truyen Pham³, Thi Giang Ha^{3,5}, Quoc Van Dinh³, Vinh Long Ha^{1,2,3}, Grigorios Lavrentiadis⁶ , Chung-Han Chan^{2,7,8} , and Dinh-Hai Pham⁹

Abstract

It is challenging to select ground motion models (GMMs) for seismic hazard assessments for a region with sparse recorded data. In this study, data on the 2020 Mw5.0 Moc-Chau earthquake and its aftershocks were used to select an appropriate GMM for northern Vietnam (NVN). The 204 strong motion records were collected from 32 seismic stations and then used to compare eleven non-Vietnamese and two simplified Vietnamese local GMMs to assess their model prediction efficiencies. Among all the candidates, the global NGA-West2 GMMs performed the best fit with the data. Our analyses revealed the possibility of damage resulting from shaking in the Hanoi metropolitan area caused by recognized earthquake sources in NVN. In our examination of total residuals of differences between the GMM predictions and observed data, the average standard deviation from ASK14 was

¹Institute of Earth Sciences, Academia Sinica, Taipei, Taiwan

²Taiwan International Graduate Program Earth Sciences System (TIGP-ESS), Academia Sinica, Taiwan

³Institute of Geophysics, Vietnam Academy of Science and Technology, Hanoi, Vietnam

⁴Graduate University of Science and Technology (GUST), Vietnam Academy of Science and Technology

⁵Hanoi University of Mining and Geology, Vietnam

⁶California Institute of Technology, Pasadena, CA

⁷Earthquake-Disaster & Risk Evaluation and Management (E-DREaM) Center, National Central University, Taoyuan, Taiwan

⁸Department of Earth Sciences, National Central University, Taoyuan, Taiwan

⁹Department of Steel Structure, Hanoi University of Civil Engineering, Vietnam

Corresponding author:

Van-Bang Phung, Institute of Earth Sciences, Academia Sinica, No. 128, Section 2, Academia Rd, Nangang District, Taipei, 11529, Taiwan.

Email: phungvb@earth.sinica.edu.tw

slightly higher than the limit accepted for modern seismic hazard assessments. ASK14 was further adjusted by the spatially varying coefficients that were derived from observations ground motion of this event. The adjusted ASK14 was used to evaluate seismic risk scenarios of large earthquakes in NVN and compared with the structures' design spectra of the Hanoi area. To increase the prediction efficiency, additional local data are required to develop a region-specific GMM for NVN. We suggest that GMM be developed in the near future by regionalizing the ASK14 GMM according to additional local data further collected from existing broadband seismic observations and new accumulating continuous recording data from Vietnam's broadband seismic networks.

Keywords

Moc-Chau earthquake, H/V ratio, GMMs' evaluation, adjusted GMM, and deterministic hazard analysis

Date received: 6 July 2023; accepted: 18 July 2024

Introduction

An earthquake with a magnitude (M_w) of 5.0 occurred near the Moc-Chau district in the northwest region of Vietnam on July 27, 2020 (Nguyen et al., 2022a; referred to herein as the 2020 Moc-Chau earthquake; Figure 1a), and this is the only significant recorded event since the seismic station networks have been installed in 2009 (Huang et al., 2009). This event has caused considerable damage to the infrastructure in the vicinity of the epicenter. Although the magnitude was moderate, people reported feeling strong shaking in the high-rise buildings of Hanoi, approximately 100 km away from the epicenter. This low-frequency shaking had not been previously reported and emphasizes the importance of the seismic hazard assessment of the potential damage of future large earthquakes in Vietnam.

In northern Vietnam (NVN), the tectonic setting categorized as a stable continental region has generally been governed by major tectonic events in the surrounding areas since the Tertiary period (Tapponnier et al., 1982). Many studies of the tectonics of NVN have assessed the seismic hazard of the region (Huang et al., 2009; Lap, 1991; Nguyen et al., 2019; Pailoplee and Choowong, 2014; Phuong, 1991). Earthquakes in NVN are characterized as shallow with focal depths ranging from 0 to 35 km (Nguyen and Le, 2005; Nguyen et al., 2019; Nguyen et al., 2022). Destructive earthquakes with maximum magnitudes of $M_{6.0}$ or greater have occurred in NVN (Das, 2015; Duan et al., 2013; Robinson et al., 2010), two of which occurred in the last century (Figure 1a): the 1935 Dien Bien earthquake, which had a surface wave magnitude (M_s) of 6.8, and the 1983 Tuan Giao earthquake, which had an M_s of 6.7. Both earthquakes caused significant infrastructural damage and economic loss (Duong et al., 2013; Tuyen and Lu, 2012).

To evaluate seismic hazards in a specific region, probabilistic seismic hazard analysis (PSHA) that incorporates source, path, and site conditions is required. Ground motion models (GMMs), named as ground motion prediction equations (GMPEs) in previous publications, are used to develop predictions of ground motion and its associated uncertainty at any location as a function of magnitude, distance, and other parameters, including style of faulting and site condition. GMMs are used to calculate the required input parameters for PSHA. In PSHA, multiple GMMs are often combined within a logic tree to quantify the ground motion uncertainty, especially for locations that lack region-specific

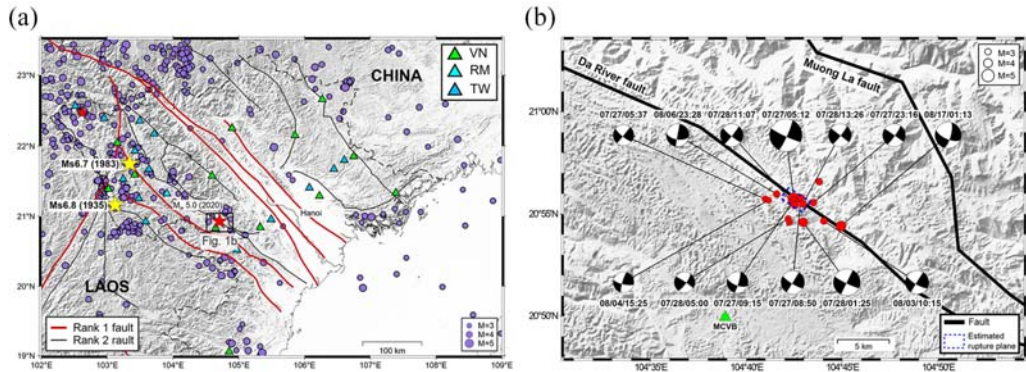


Figure 1. (a) Map of seismicity in the northern Vietnam from 1990 to 2021. White symbols denote seismic stations from four different networks: Vietnam National network (VN), Academia Sinica-Taiwan (TW; Huang et al., 2009), the Regional Integrated Multi-Hazard Early Warning System (RM), and Pacific21 (PS). Each station code is listed below its respective symbol. Regional active faults are marked as thick red lines (rank I major faults) and solid thin black lines (rank II minor faults; Nguyen et al., 2019). The red star symbol represents the epicenter of the 2020 Moc-Chau earthquake, and the yellow star symbols represent the locations of the events discussed in this study. (b) The event distribution of the 2020 Moc-Chau earthquake sequence and its focal mechanisms (Nguyen et al., 2022a). The date and time of each event are listed next to its focal mechanism. The location of Figure 1b is marked as a box surrounding the epicenter in Figure 1a.

GMMs (Bommer, 2012). Therefore, an appropriate suite of GMMs is usually selected according to models developed for similar tectonic regions (Bommer et al., 2005). Recent PSHA studies have attempted to identify the optimal suite of GMMs that includes both global and region-specific (for major tectonic environments) components (GeoPentech, 2015; Phung et al., 2018).

In respond to the urbanization and construction of large public facilities in Vietnam, various seismic hazard reduction measures, including the selection of suitable GMMs, have been proposed (Nguyen et al., 2012; Tran and Kiyomiya, 2012, 2013). Since then, new evaluation techniques have been developed and high-quality earthquake data have been collected, and the GMMs for Vietnam must be reviewed and updated accordingly. The updated GMMs should be developed with reference to local data; however, to date, only limited onsite observations are available. A suitable approach to this problem is to systematically evaluate the applicability of GMMs from other regions by using what limited set of high-quality local observations there are, as is commonly done by earthquake engineers in other parts of the world when the study region exhibits low seismicity or when limited seismic data are available for the region (Nizamani and Park, 2021; Ornthammarath et al., 2020). To verify the prediction efficiencies of a selected GMM, a testing with extra available data is helpful. In this study, we used the high-quality strong ground motion data from the 2020 Moc-Chau earthquake sequence to evaluate the selection of GMMs for NVN and raise several issues for discussion.

Observation of the 2020 Moc-Chau earthquake sequence

The Moc-Chau earthquake occurred with moment magnitude (M_w) of 5 at 05:15 (UTC; local time: 12:15) on July 27, 2020. The hypocenter of the mainshock had a depth of 7 km and was located at 20.929°N, 104.708°E, approximately 12 km away from the town of

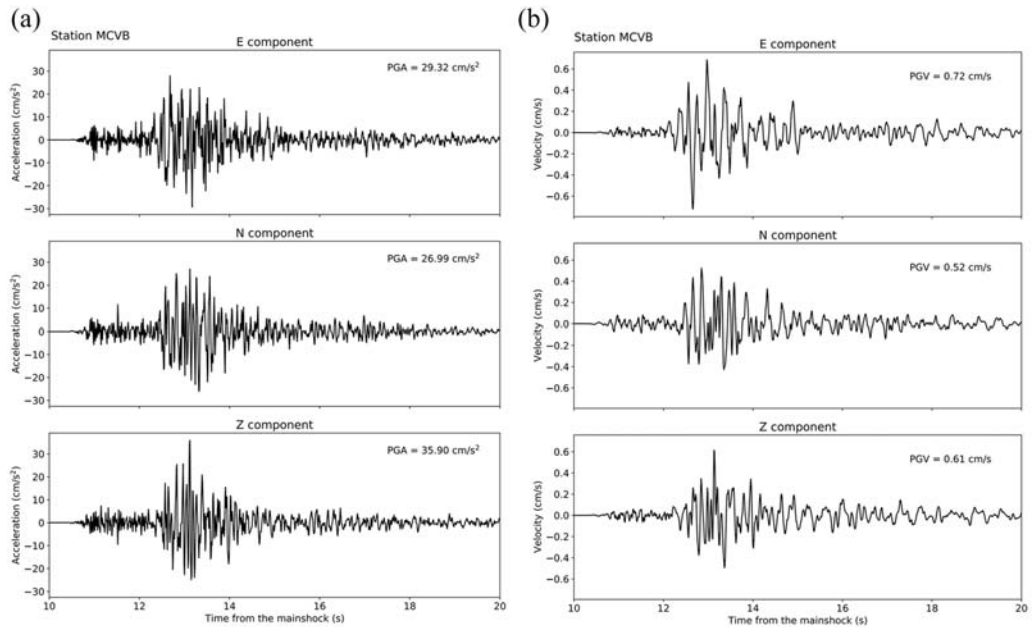
Moc-Chau (Figure 1a). Table 1 displays the details of main shock and its aftershocks regarding location of epicenter and source-related parameters such as magnitude (M_w) and depths (H). The earthquake severely damaged the infrastructure in the vicinity of the epicenter (Nguyen et al., 2022a). During the earthquake, people felt strong shaking in the near-source region and in some tall buildings in the nearby cities. On the United States Geological Survey response website for earthquakes (Wald et al., 2012), 31 local witnesses responded to the question “Did you feel it?” for the Moc-Chau earthquake. Some descriptions of shaking, mostly from high-rise buildings in Hanoi, were classified as level III according to the Medvedev-Sponheuer-Karnik scale (Medvedev and Sponheuer, 1969), which is similar to modified Mercalli intensity scale. Numerous aftershocks followed the mainshock, all of which were concentrated in a small region (Figure 1b). Two large aftershocks with magnitudes >4 occurred on July 28 ($M_w = 4.1$) and August 17 ($M_w = 4.4$) (Table 1). The ground motions of the events were recorded by 32 broadband seismic stations in NVN (Figure 1a). The stations belonged to three networks: Vietnam National Network (VN); Academia Sinica, Taiwan (TW) (Huang et al., 2009); and the Regional Integrated Multi-Hazard Early Warning System (RM). Each VN and RM station was equipped with an accelerometer and a broadband velocity seismometer (Lu et al., 2018; Nguyen et al., 2012). The nearest VN seismic station, station MCVB, was located in the town of Moc-Chau, 12.4 km away from the mainshock epicenter (Figure 1a). According to a report on the earthquake sequence (Nguyen et al., 2022a), the focal mechanisms of the events examined herein were strongly affected by strike-slip movements. The seismicity pattern and source mechanism from the moment tensor inversion analysis reveal that the earthquake sequence might have been associated with the active right lateral Da River fault (Figure 1b).

In this study, we selected 204 high-quality records from all 32 broadband seismic stations in NVN that were continuously collecting data during the Moc-Chau earthquake sequence (Figure 1a). The mainshock ($M_w = 5.0$) and its aftershocks with magnitudes >3.0 (13 events, as indicated in Table 1) were considered in our analysis. Figure 2a presents the record in the time domain of the three-component accelerations caused by the mainshock at station MCVB, approximately 12 km away from the epicenter. The peak peak ground motion accelerations (PGA) observed at this station were 35.9, 29.3, and 26.7 cm/s^2 in the vertical, east–west (E–W), and north–south (N–S) components, respectively. The maximum peak ground velocity (PGV) derived from the integration of the acceleration time histories in the E–W component was weak (0.72 cm/s ; Figure 2b). Detailed information of the data used in this study and its validations is presented in Phung et al. (2024) and the Supplementary Material (Appendix A).

Traditionally, acceleration and velocity sensors were operated by different seismic networks for different purposes. A strong-motion seismic network stations equipped with accelerometers operated in trigger mode with low sensitivity to record strong ground accelerations from large-magnitude earthquakes or near source events, whereas regional network seismic stations equipped with bandlimited velocity seismometers operated using a continuous model with high sensitivity were deployed to record low ground velocities from small local earthquakes or teleseismic events. By contrast, in a modern broadband station, signals from both the accelerometer and the broadband velocity sensor are continuously recorded at the same site and share the same data logger. Figure 3 presents an example of the waveforms of the velocity (Figure 3a) and acceleration (Figure 3b) in the N–S component from the mainshock that were recorded at station MCVB. After the instrument response is excluded, the broadband velocity seismogram is then simply

Table 1. List of Moc-Chau earthquakes and source-related parameters.

Event name	M_w	R_{hyp} range km	Location	Depth (km)	Number of records
202007270514 (Main shock)	5	14.3–282	20.929°N 104.708°E	8.1	31
202007270537	3.1	12.2–182	20.929°N 104.683°E	7	8
202007270915	3.2	10.8–282	20.928°N 104.708°E	6.0	13
202007272316	3.4	11.2–279	20.926°N 104.725°E	1.0	15
202007280125	4.1	12.3–282	20.910°N 104.716°E	5.3	32
202007280500	3.1	11–275	20.913°N 104.703°E	7.2	10
202007281107	3.4	10.3–283	20.925°N 104.708°E	10	14
202007281326	3.5	12–280.1	20.925°N 104.716°E	6.1	14
202008031015	3.4	14.1–251	20.911°N 104.734°E	6.6	10
202008062328	3	11.1–275	20.933°N 104.693°E	10	13
202008170113	4.4	13.4–278	20.907°N 104.749°E	8.1	28
202007270850	3.4	13–280	20.930°N 104.714°E	7.0	13
202008041525	3.4	13.5–282.1	20.928°N 104.686°E	10.1	6

**Figure 2.** Three-component recordings of corrected acceleration (a) and velocity integrated from acceleration (b) of the 2020 Moc-Chau earthquake, as recorded by station MCVB.

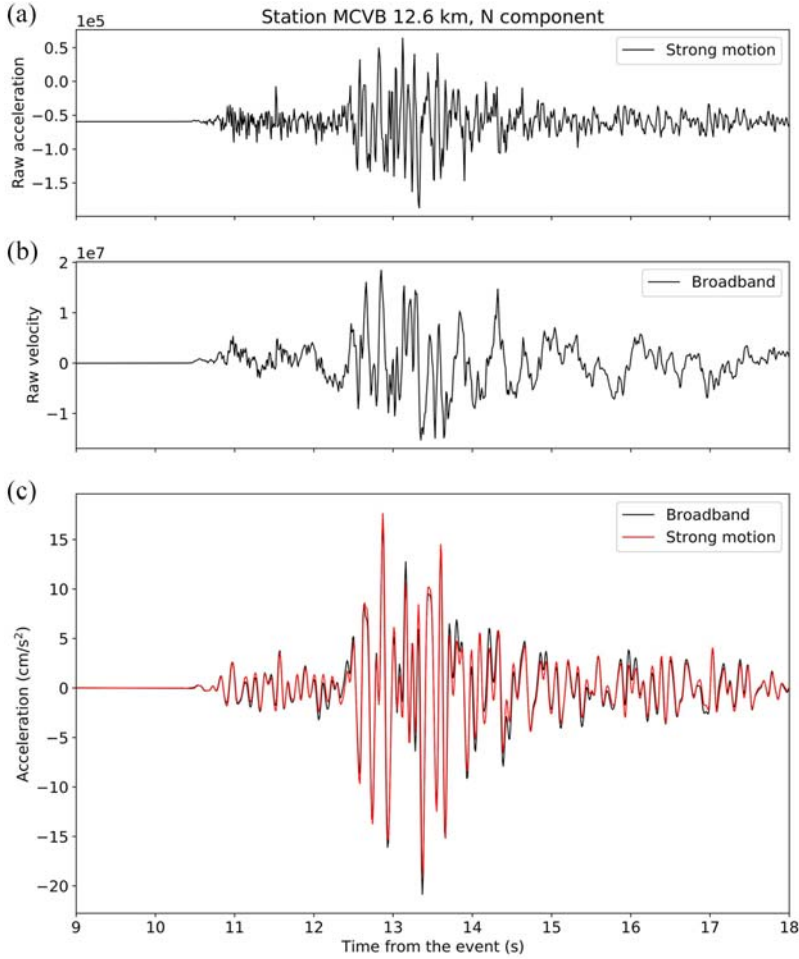


Figure 3. The raw N-S component recordings from the accelerometer (a) and the broadband velocity seismometer (b) of station MCVB. (c) Comparison of the instrument response-corrected accelerations from the broadband velocity seismometer and accelerometer.

differentiated to derive the corresponding acceleration, which can observe to be similar with the accelerogram presented in Figure 3c. The combined broadband velocity and acceleration exhibit a large dynamic range with respect to the recorded ground motion. This implies that the broadband network may record extra data, such as recordings for distant large events or smaller local events untriggered by the independent strong ground accelerations, for use in earthquake engineering.

The raw data was processed using a methodology similar to that of Elomo et al. (2015). The waveforms of each station-event pair were applied mean and trend removal, instrument response removal, and band-pass filtered in the frequency between 0.1 to 20 Hz by a zero-phase shift four-pole Butterworth filter. The waveforms were then cut into windows containing the event. In our study, we use a uniform scheme for all records and only select the waveforms with a signal-to-noise of at least 5. We estimate the P-wave arrival using $P_{\text{PHASEPICKER}}$ algorithm (Kalkan, 2016). The noise and earthquake signal can then be

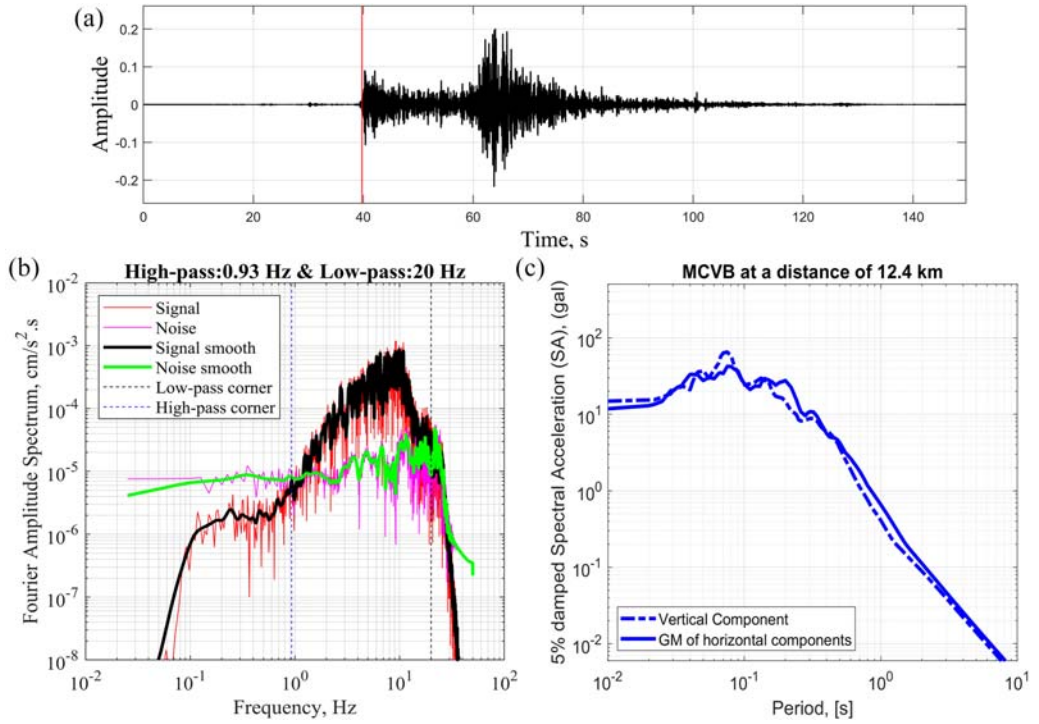


Figure 4. (a) An example of recorded ground motion and selected noise recorded ground motion (20101230185016 north-south component, at recorded at BGVB by an event $M_w = 4.4$), and (b) Illustrative plot for selecting filter corner frequencies (low-pass and high-pass corner frequency). (c) The 5% damped pseudo-spectral acceleration (SA) of the MCVB station plotted against the natural period of the single-degree-of-freedom system for the vertical component (dashed line) and the geometric mean (GM) of the two horizontal components (solid line).

identified in the acceleration time histories (Figure. 4a), and this allows for the computation of the signal to noise ratio (SNR) used to assess the quality of ground motion recordings. The filter corner is determined by comparing the Fourier amplitude spectra (FAS) of ground motion recordings with that of the noise window, as shown in Figure 4b. The filter frequencies were selected to minimize the residual deformation in the residual deformation; the minimum usable frequency as set as 1.20 times the lower high-pass frequency of filtering for each record.

In seismic hazard analysis and earthquake engineering, the pseudospectral acceleration (SA) of a 5% damped single-degree-of-freedom (SDOF) oscillator is commonly used as an intensity measure for the dynamic response of a wide range of structures. In this study, we calculated the PGA and 5% damped SA for 105 periods of 0.01 to 10 s for each component of a time series. The observed horizontal motion was converted into the geometric mean (GM) of the two individual horizontal components. As indicated in Figure 4c, the 5% damped SA for station MCVB was associated with the time series in Figure 2a. For the period < 0.1 s, the 5% damped SA values of the vertical component were larger than the GM of the horizontal components, which implies that the vertical ground motion can strongly affect the seismic response of structures located near the source region. Such

vertical effects are observed to be consistent with the findings in other previous studies (e.g., Bozorgnia & Campbell, 2016; Phung et al., 2022).

Evaluation of existing GMMs

In this study, a set of worldwide developed GMMs were selected for NVN to assess the seismic hazards. Performing seismic hazard analysis for a region requires estimations of ground motion distribution in terms of magnitude, distance, and site condition as inputs. As a part of the selection process of the GMMs for NVN, we examined the ground motion characteristics of selected events, as described in Table 1, by comparing the observed ground motion (PGA and PSA) with those predicted by a number of selected GMMs based on equations formulated for Vietnam and for other regions (Table 2). The main characteristics of Vietnamese GMMs are compared with those of non-Vietnamese GMMs, which are listed in Table 2.

Ground motion inputs

The source parameters of moment magnitude (M_w), focal depth (H), and the hypocentral (or epicentral) distance were used as inputs for the GMMs and compared the results with the ground motion observed during the Moc-Chau earthquake sequence. Because the magnitudes of all the events in the earthquake sequence were low ($M_w = 5.0$ for the mainshock and $M_w < 5.0$ for the aftershocks), the point source model was adopted. Therefore, (a) the hypo-central distance (R_{hyp}) was equal to the rupture distance (R_{rup}) and (b) the epicentral distance (R_{epi}) was equal to the Joyner–Boore distance (R_{jb}). In addition, the focal depth (H) was equal to the depth to the top of the rupture (Z_{tor}), and the style of faulting (sof) was set to vertical strike-slip that is consistent with focal mechanism of the considered events.

Vietnamese GMMs

Early studies on the development of region-specific GMMs for NVN were based on the attenuation equations of Nguyen et al. (2012, hereafter N12) and Tran and Kiyomiya (2012, hereafter TK12). Due to their simple functional forms, neither GMM has been used for modern seismic hazard assessment in Vietnam. However, these two GMMs are useful for studying PGA attenuation. Figure 5 presents the observed ground motion and the predicted ground motion results of the N12 GMM (solid curve) and TK12 GMM (dashed curve) for comparison. Comparisons were drawn between the predicted and observed values for the Moc-Chau mainshock (Figure 5a), the two aftershocks with magnitudes >4.0 (Figure 5c), and other aftershocks with magnitudes >3.0 (Figure 5c). The epicentral distance of the mainshock measured at station MCVB was 12.4 km, and all the aftershocks clustered around the mainshock (Figure 1). The observed PGAs reflected clear epicentral distance attenuation for the mainshock and aftershocks. The ground motion predicted by the N12 GMM was generally consistent with its observed counterpart for all the selected events. The predictions of TK12 GMM for the same events were significantly greater than those of the N12 GMM (Figure 5).

Although the N12 GMM and TK12 GMM fit the data, these models have some limitations. The model was developed using the epicentral distance and does not account for site conditions (such as rock and soil). In addition, the local Vietnam GMMs use a common linear magnitude scaling term that can potentially lead to an overprediction for large

Table 2. General features of the worldwide GMMs compared with the Northern GMMs.

Abbreviation GMMs	The tectonic environment	Period range	M-range	R-range (km)	Site condition	Style of faulting	Applicable region	Sigma (LN)
Nguyet et al. (2012, NI2)	Stable continental	PGA	$M_L = 3.0-5.0$	$R_{hyp} = 10-200$	None	None	Vietnam	0.687
Tran and Kiyomiya (2012, 2013, TK12)	Stable continental	PGA	$M_L = 3.0-5.0$	$R_{hyp} = 10-200$	None	None	Vietnam	0.702
Campbell and Bozorgnia (2008, CB08)	Shallow crustal	PGA and Sa at 0.01 to 10 s	$M_W = 4.0-8.5$	$R_{RUP} = 0-200$	V_{S30}	RV, SS, NM	Global	0.563–0.957
Akkar et al. (2014, ASB14)	Shallow crustal	PGA and Sa at 0.01 to 4 s	$M_W = 4.0-7.5$	$R_{JB} = 0-300$	V_{S30}	RV, SS, NM	Europe and Middle East	0.567–0.882
Abrahamson et al. (2014, ASK14)	Shallow crustal	PGA and SA at 0.01 to 10 s	$M_W = 3.0-8.5$	$R_{RUP} = 0-300$	V_{S30} and $z_{1.0}$	RV, SS, NM	Global	0.683–0.889
Boore et al. (2014, BSSA14)	Shallow crustal	PGA and SA at 0.01 to 10 s	$M_W = 3.0-8.5$	$R_{JB} = 0-400$	V_{S30} and $z_{1.0}$	RV, SS, NM, U	Global	0.605–0.942
Campbell and Bozorgnia (2014, CB14)	Shallow crustal	PGA and SA at 0.01 to 10 s	$M_W = 3.0-8.5$	$R_{RUP} = 0-300$	V_{S30} and $z_{2.5}$	RV, SS, NM	Global	0.583–0.928
Chiou and Youngs (2014, CY14)	Shallow crustal	PGA and SA at 0.01 to 10 s	$M_W = 3.5-8.0$	$R_{RUP} = 0-350$	V_{S30} and $z_{1.0}$	RV, SS, NM	Global	0.681–0.835
Chao et al. (2020, Ch20)	Shallow crustal	PGA and SA at 0.01 to 5 s	$M_W = 3.5-7.6$	$R_{RUP} = 0-400$	V_{S30} and $z_{1.0}$	RV, SS, NM	Taiwan	0.613–0.889
Phung et al. (2020, Ph20)	Shallow crustal	PGA and SA at 0.01 to 10 s	$M_W = 3.5-8.0$	$R_{RUP} = 0-300$	V_{S30} and $z_{1.0}$	RV, SS, NM	Taiwan	0.625–0.902
Atkinson and Boore (2006, AB06)	Stable continental	PGA and SA at 0.01 to 10 s	$M_W = 3.0-8.5$	$R_{RUP} = 1-1000$	$V_{S30} > 3000$ m/s	Not explicitly considered	CENA	0.6908
PEER (2015)	FAS-based RVT Convert	FAS-based RVT convert	$M_W = 3.0-8.0$	$R_{RUP} = 0-500$	V_{S30}	Not explicitly considered	CENA	NA
Emolo et al. (2015, E15)	Stable continental	PGA and SA at 0.01 to 5 s	$M_W = 2.0-5.0$	$R_{EPI} = 2-1000$	Dummy variable	Not explicitly considered	Korea	0.71–0.89

events (e.g., M7), thus overpredicting the hazard events or large events dominating the hazard deaggregation (GeoPentech, 2015; Phung et al., 2018). In fact, these equations should not be used in PSHA according to the exclusion criteria proposed by Bommer et al. (2010). Moreover, neither the N12 nor the TK12 GMM accounted for long-period predictions, which is a major limitation in modern seismic hazard assessment and in earthquake engineering. Therefore, an appropriate selection of the worldwide GMMs or a new GMM must be conducted for the NVN region, potentially through the refinement of a GMM from another region.

Non-Vietnamese GMMs

Modern GMMs enable comprehensive analyses of ground motion at different periods. In this study, the geometric mean of ground motion for the PGA and 5% damped PSA were examined at 0.2 and 1.0 s. In this study, the choice of potential GMMs will be tested for areas with poorly known seismological characteristics and few available recorded motions. Due to these challenges, 11 GMMs from both the stable continental areas and the active crustal regions were chosen for the evaluation. We categorized 11 candidate GMMs into four groups. The first group of four equations (Abrahamson et al., 2014 [ASK14]; Boore et al., 2014 [BSSA14]; Campbell and Bozorgnia, 2014 [CB14]; Chiou and Youngs, 2014 [CY14]) was developed for global application as part of the Next Generation Attenuation Relationships for the Western United States (NGA-West2) project (Bozorgnia et al., 2014). The second group comprised two Taiwan-specific regional GMMs (Chao et al., 2020 [Ch20]; Phung et al., 2020 [Ph20]) developed for PSHA in Taiwan (NCREE, 2015; Phung et al. 2018). The third group comprised two equations (Campbell and Bozorgnia, 2008 [CB08]; Akkar et al., 2014 [ASB14]) that were used in recent PSHA studies in Vietnam (Pham and Nguyen, 2019). The three groups represent the active crustal regions from the United States and Taiwan. The final group representative the stable continental areas from Central East North America (CENA) and Korea. This group comprised three equations (Atkinson and Boore 2006 [AB06]; Elomo et al., 2015 [E15]; PEER (2015)). The general features of the selected candidate GMMs are summarized in Table 2, the horizontal-component definitions, the associated lognormal standard deviation, and the applicable range are specified. It is worth emphasizing that CB08 differs from other GMMs as it is meant to predict the near field data and did not include an anelastic attenuation term.

Estimation of V_S^{30}

For the implementation of most of the GMMs listed, the shear wave velocity in the upper 30 m (V_S^{30}) is commonly used as a parameter for describing the site conditions. However, the measurement of V_S^{30} is not available for the seismic stations under consideration in this study. Given such conditions, we referred to the deduced site conditions based on the predominant period (T_g) – V_S^{30} correlation relationship proposed by Hassani and Atkinson (2016) (as shown in Equation 1)

$$\log_{10}(V_S^{30}) = \begin{cases} 2.2(\pm 0.04) + 0.63(\pm 0.06)\log_{10}\left(\frac{1}{T_g}\right) & \text{for } T_g < 0.5s \\ \log_{10}(250) & \text{for } T_g \geq 0.5s \end{cases} \quad (1)$$

This equation was proposed for Center East North America (CENA) region in which the T_g value is the period corresponding to the peak (P^*) of the horizontal to vertical spectra

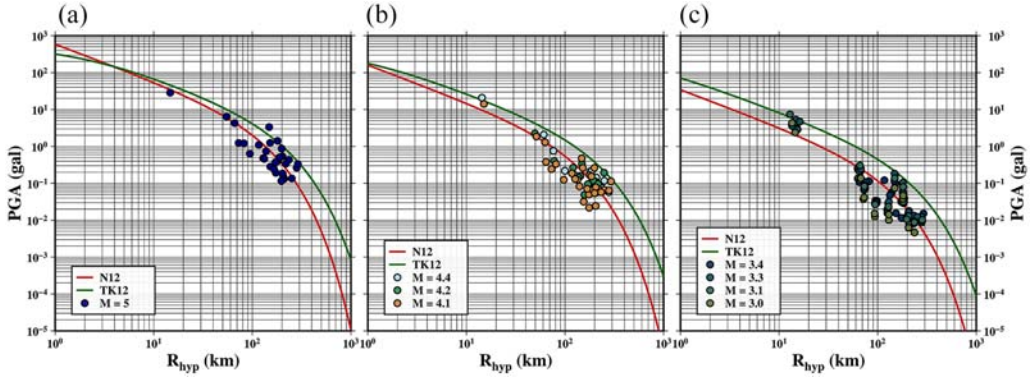


Figure 5. Comparison of observed ground motion for PGA and those estimated using the N12 (green curve) and TK12 (red curve) GMMs: (a) Moc-Chau mainshock ($M_w = 5.0$), (b) the three $M_w \geq 4$ aftershocks, and (c) the other aftershocks ($M_w \geq 3$). Horizontal axis represents the epicentral distance. The nearest station (epicentral distance) to each event was station MCVB.

ratio (HVS_R), which was defined by Nakamura (1989) and later used for proposing site classification schemes in several studies (Di Alessandro et al., 2012; Mercado et al., 2023; Zhao et al., 2006). The HVS_R for each record was first computed as the geometric mean of the response spectra of the two horizontal components divided by the response spectra of the corresponding vertical component. Then the HVS_R for each station was averaged over the individual HVS_R of that station (with at least three recordings). Figure 6a shows an illustrative example of average HVS_R plotted against periods for three seismic stations in which the T_g and P^* values are identified for 31 stations.

For T_g greater than 0.5 s, corresponding to sites with deep sediments (sediments deeper than 30 m), the average value is anchored 250 m/s because V_S^{30} for this site does not provide any information from the deeper sediment layers. The T_g – V_S^{30} relationship is independent of P^* , which might lead to the sites having low V_{S30} but flat HVS_R. A site with flat HVS_R with P^* smaller than 2.0 was classified as rock-stiff soil according to Di Alessandro et al. (2012). We subjectively constrained the flat HVS_R sites ($P^* < 1.5$) to be rock ($V_S^{30} = 1500$ m/s). As a result, Figure 6b shows a plot of inferred V_S^{30} compared with the topographic slope V_{S30} (USGS available). Table 3 lists the peak of HVS_R values (P^*), the corresponding predominant period (T_g), and the inferred V_S^{30} as well as the topographic slope V_S^{30} for each seismic station.

According to Hassani and Atkinson (2016), the uncertainty of the estimated V_S^{30} varies from 0.14 (log₁₀ unit) to 0.25 (log₁₀ unit) depending on the dominant period (T_g). This uncertainty could be larger when applying the CENA's equation to the northern Vietnam region. The additional uncertainty is due to the difference in T_g or the geological site condition of the study region from which the region of the adopting equation was proposed. This uncertainty can translate into errors in the assumed site amplification and hence increased ground motion variability for the applying region. However, this uncertainty can be estimated in the future by implementing V_{S30} measurements and applying ambient-noise studies for sites. On the other hand, there is a possible bias on estimated V_S^{30} value, which may impact the GMMs predictions. We analyze the impact of V_S^{30} on the predictions of selected GMMs by examining the correlation coefficient between site term obtained from a GMM with $V_S^{30} = 1000$ m/s (hard rock) and the natural logarithm of V_S^{30} (i.e., $\ln(V_S^{30})$).

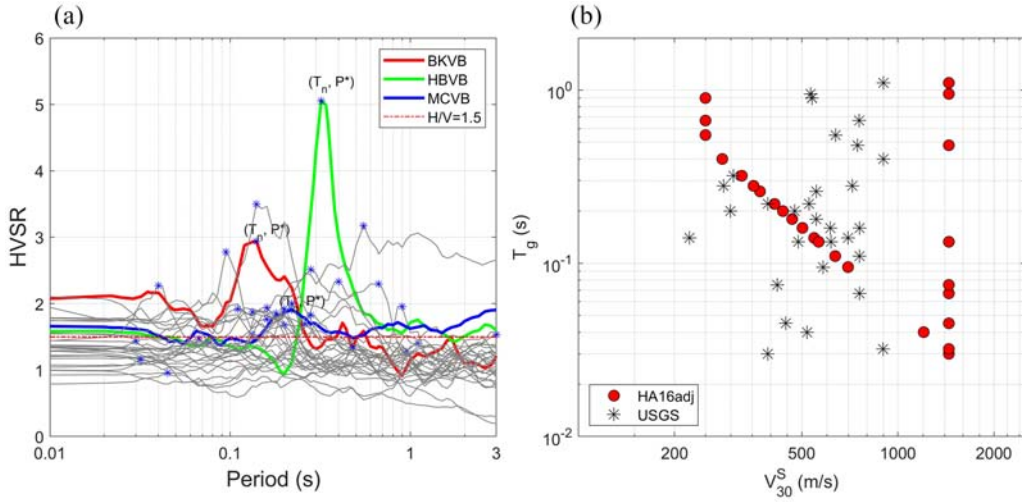


Figure 6. (a) An illustrative example of determining the predominant period (T_g) and peak of HVSR (P^*) for three seismic stations (BKVB, HBVB, and MCVB). (b) A plot of inferred V_{30} , obtained from the T_n – V_{30} relation of Hassani and Atkinson (2016b), as a function of predominant period (T_n).

Conceptually, the larger correlation coefficient indicates that the associated GMM has a greater capacity for adapting the inferred V_{30} for its prediction. In other words, the higher correlation coefficient given to a GMM, the inferred V_{30}^{30} is more consistent with the GMM's site response model. The site term of each GMM was derived by using mixed effect regression algorithm (Bates et al. 2014). Then the GMMs' residuals (δ_{es}) can be partitioned into between-event (δB_e) and within-event residual (δW_{es}).

$$\delta_{es} = \ln(y_{es}) - f(M, R, V_{30}^{30} = 1000, \dots) = \delta B_e + \delta W_{es} \quad (2)$$

where index e refers to an earthquake e^{th} and index s refers to station s^{th} . The quantity y_{es} is an observed spectral acceleration; $f(\dots)$ is the GMMs' predicted rock motion. Figure 7 shows the correlation coefficient values plotted against the period for each GMM. The correlation coefficients are mostly negative, which indicates that the rock within-event residual has a negative trend with V_{30}^{30} . This represents a physical property where soil sites can have larger site amplification than rock sites. It appears that the correlation coefficients exhibit negative values ranging from -0.3 to -0.45 in short periods ($T < 0.75$ s), whereas they show smaller negative values ranging from -0.1 to -0.2 in long periods ($T > 0.75$ s). In particular, three models from the CENA and Japan regions (AB06, HB22, and Zh06) represent relatively large correlation values, while the NGAWest2 GMMs represent moderate to high correlation values. On the other hand, two specific Taiwanese models appear to have low correlations, where the inferred V_{30}^{30} is not suitable to model the site response in their modeling. The range of correlation coefficient values can be considered as epistemic uncertainty in predicting site amplification for the study region. Note that HB22 performs a positive correlation at long $T = 3.0$ s. This behavior is not usually seen in most GMMs and should be examined further when the measurement of V_{30}^{30} is available.

Table 3. List of 31 stations for inferred V_{S30} values. The peak (P^*), the predominant period (T_g), and NEHRP site class are also identified for each station.

Station code	Peak of H/V ratio	Dominant period, T_g (s)	Zhao et al. (2006) & Alessandro et al. (2012) classification	NEHRP class	Hassani and Atkinson, (2016) suggested V_{S30} (m/s)	USGS referenced V_{S30} (m/s) (Health et al., 2020)	Note
BKVB	2.937	0.140	SC-I: rock stiff soil	A + B + C	547 ± 202	223	
CBVB	1.534	3.000	SC-I: rock stiff soil	A + B + C	1443 ± 533	713	Flat H/V and peak < 2
CCVB	1.398	1.100	SC-I: rock stiff soil	A + B + C	1443 ± 533	900	Flat H/V
DBVB	2.298	0.667	SC-IV: soft soil	D + E	250 ± 92	757	
HBVB	5.052	0.320	SC-II: hard soil	C + D	325 ± 120	306	
HGVB	1.958	0.900	SC-IV: soft soil	C + D	250 ± 92	539	
LSVB	1.470	0.067	SC-I: rock stiff soil	A + B + C	1443 ± 533	759	Flat H/V
MCVB	1.907	0.220	SC-II: hard soil	C + D	411 ± 152	392	Peak < 2
MLAV	1.764	0.160	SC-I: rock stiff soil	A + B + C	503 ± 186	615	Peak < 2
MLVB	1.697	0.260	SC-II: hard soil	C + D	370 ± 137	556	Peak < 2
SLV	1.277	0.950	SC-I: rock stiff soil	A + B + C	1443 ± 533	534	Flat H/V
TGVB	1.677	0.200	SC-II: hard soil	C + D	437 ± 161	475	Peak < 2
THVB	1.415	0.075	SC-I: rock stiff soil	A + B + C	1443 ± 533	419	Flat H/V
TYVB	3.498	0.140	SC-I: rock stiff soil	A + B + C	547 ± 202	699	
VCVB	2.001	0.220	SC-II: hard soil	C + D	411 ± 152	527	Multiple peaks
VN01	2.331	0.400	SC-III: medium soil	D	282 ± 104	900	
VN03	3.170	0.550	SC-III: medium soil	D	250 ± 92	638	
VN04	2.781	0.095	SC-I: rock stiff soil	A + B + C	698 ± 258	583	Flat H/V and peak < 2
VN08	1.874	0.133	SC-I: rock stiff soil	A + B + C	565 ± 208	617	Flat H/V
VN09	1.435	0.030	SC-I: rock stiff soil	A + B + C	1443 ± 533	392	Flat H/V
VN10	1.347	0.480	SC-I: rock stiff soil	A + B + C	1443 ± 533	747	Flat H/V
VN11	1.853	0.180	SC-I: rock stiff soil	A + B + C	467 ± 172	556	Flat H/V and peak < 2
VN12	0.957	0.045	SC-I: rock stiff soil	A + B + C	1443 ± 533	446	Flat H/V
VN14	1.534	0.133	SC-I: rock stiff soil	A + B + C	1443 ± 533	488	Flat H/V and peak < 2
VN15	1.158	0.032	SC-I: rock stiff soil	A + B + C	1443 ± 533	899	Flat H/V
VR03	1.917	0.200	SC-II: hard soil	C + D	437 ± 161	299	Clear peak and peak < 2
VR05	2.513	0.280	SC-II: hard soil	C + D	353 ± 130	285	
VR10	1.830	0.280	SC-II: hard soil	A + B + C	353 ± 130	720	Clear peak and peak < 2
VR18	2.272	0.040	SC-I: rock stiff soil	A + B + C	1204 ± 444	520	
VR25	1.918	0.110	SC-I: rock stiff soil	A + B + C	637 ± 235	759	Clear peak and peak < 2
VTVB	1.936	0.160	SC-I: rock stiff soil	A + B + C	503 ± 186	759	Clear peak and peak < 2

Note: According to Di Alessandro et al. (2012), a site can be classified as rock or as hard, medium, or soft soil based on the predominant period (T_g) and the peak value of the HVRS determined from seismic records; T_g can be defined as <0.2, 0.2–0.4, 0.4–0.6, and ≥ 0.6 s for rock and hard soil (SC-I), hard soil (SC-II), medium soil (SC-III), and soft soil (SC-IV), respectively.

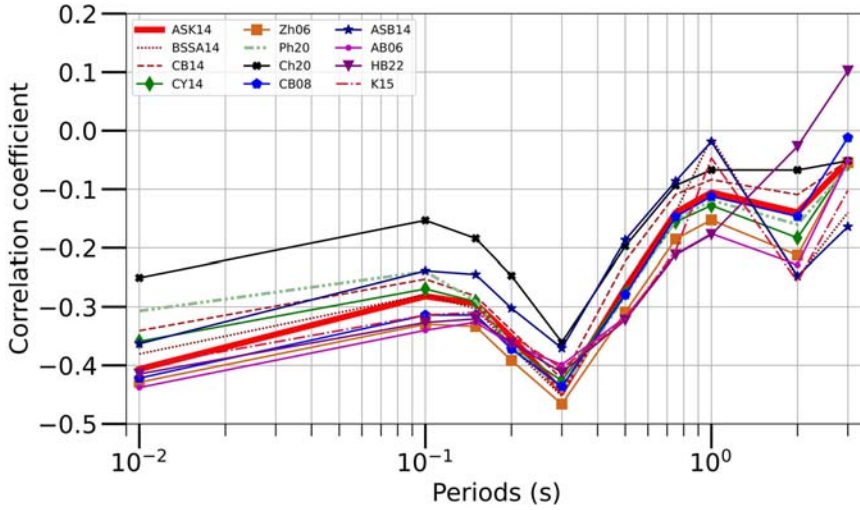


Figure 7. A plot of correlation coefficients as a function of period. Correlation between the rock within-event residual with $\ln(V_{S30})$ is computed for the selected candidate GMMs.

Models' evaluation

The ground motions predicted by the candidate GMMs and the observed PGA and SAs in the records of the selected events for periods $T = 0.2$ and 1.0 s are presented in Figure 8 for comparison. The predictions of the candidate GMMs were computed using $M_w = 5$ (upper panel) and $M_w = 3.5$ (lower panel) to compare the values for the mainshock ($M_w = 5$) and average of the aftershocks ($M_w < 4.0$). The first column illustrates the comparison of the PGAs, and the second and third columns illustrate the comparisons of the PSAs for oscillator periods of 0.2 and 1.0 s, respectively. As indicated in Figure 8, when $M_w = 5$, the average PGA and 0.2 s SA were smaller than the predictions of the candidate GMMs, especially for distances shorter than 30 km, suggesting that the data from NVN have a different distance decay rate than those from Taiwan (Ch20 and Ph20) and California (ASK14, BSSA14, CB14, and CY14). Even three GMMs (AB06, HB22, and N15) derived from the stable continental tectonic region (central and eastern North America and Korea) similar to northern Vietnam perform very different distance decay relative to the observed data. Furthermore, the predictions of the candidate GMMs had a poor fit with the observed data when the period $T = 1.0$ s. When $M_w = 3.5$, the candidate GMMs exhibited good visual fit with the observed data, even for the oscillator period of 1.0 s.

To more accurately assess the candidate models' goodness of fit, we used the log-likelihood (LLH) method proposed by Scherbaum et al. (2009) for evaluation. The LLH calculated the negative average sample by

$$LLH = -\frac{1}{N} \sum_{i=1}^N \log_2(g(x_i)) \quad (3)$$

where N is the number of observations (x_i), and $g(x_i)$ is the probability density function produced by selected GMM at x_i . The function $g(x_i)$ is calculated as

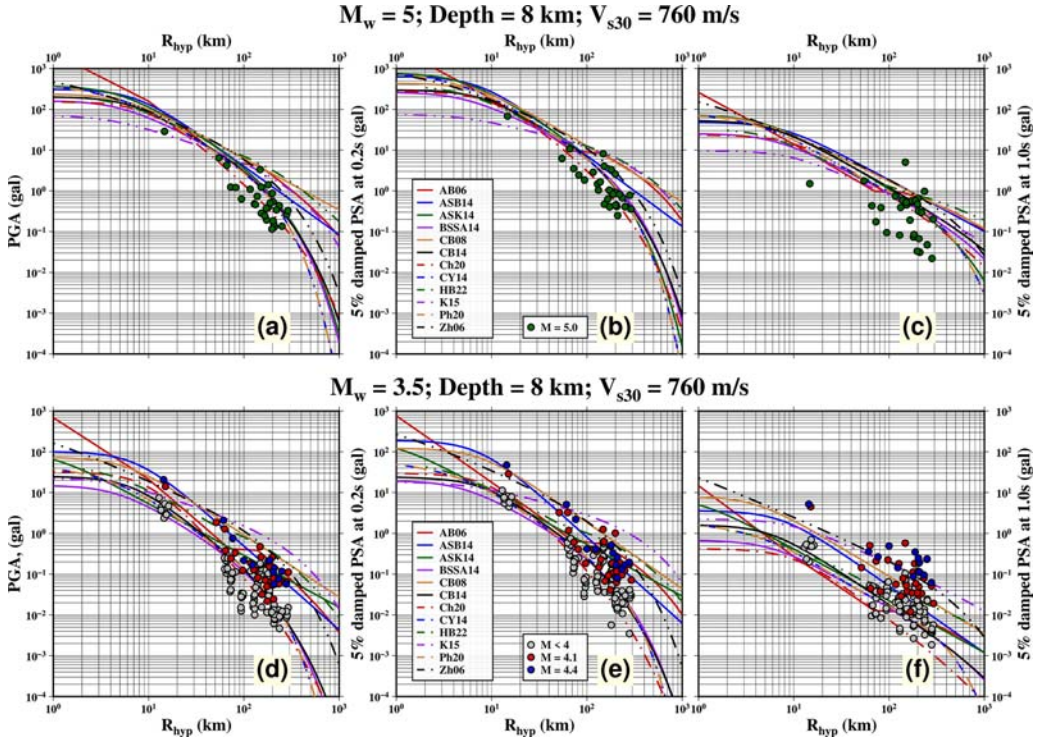


Figure 8. Comparison of predicted PGA (a and d) according to candidate GMMs and SA with period $T = 0.2$ (b and e) and 1.0 s (c and f) against observed data from selected 13 events. The candidate GMMs were computed using $M = 5$ (mainshock, upper panels) and $M = 3.5$ (average of aftershock, lower panels). The candidate GMMs accounted for vertical strike slip fault, and site parameters with $V_{s30} = 760$ m/s and $\Delta z_{1.0} = 0$ as input.

$$g(x_i) = \frac{1}{\sigma\sqrt{2\pi}} \exp\left(-\frac{(x_i - \mu)^2}{2\sigma^2}\right) \quad (4)$$

where μ and σ are median (i.e., mean the log of intensity measure) and standard deviation of the GMM model, respectively. A smaller LLH value indicates that the GMM better fits the observational data. The calculated LLH indices of all the selected candidate GMMs for 10 spectral periods between 0.01 and 1.0 s are displayed in Figure 9. The LLH values in Figure 9 indicate that CB08 fit poorly with the observed data, possibly because small-magnitude ($M < 5$) data were not considered in the development of the CB08 model. Poorly fitted models are also given to three models from the CENA and Korea regions (AB06, HB22, N15) with relatively large LLH values. The CB08 and ASB14 had lower attenuation with distance (Figure 8) than did the observed data, resulting in large LLH indices. The two Taiwan-specific GMMs (models Ch20 and Ph20) exhibited good fit with the data (up to 0.2 s) as they had relatively small LLH values. However, at higher spectral periods, LLH values of Ch20 increased (~ 3.5 at 1 s), whereas those of Ph20 decreased by almost half (~ 2.4 at 1.0 s) (Figure 9). The LLH values of the four NGA-West2 models (ASK14, BSSA14, CB14, and CY14) were smaller than those of the Taiwanese models, which indicated that the NGA-West2 models fitted the observed data more closely than

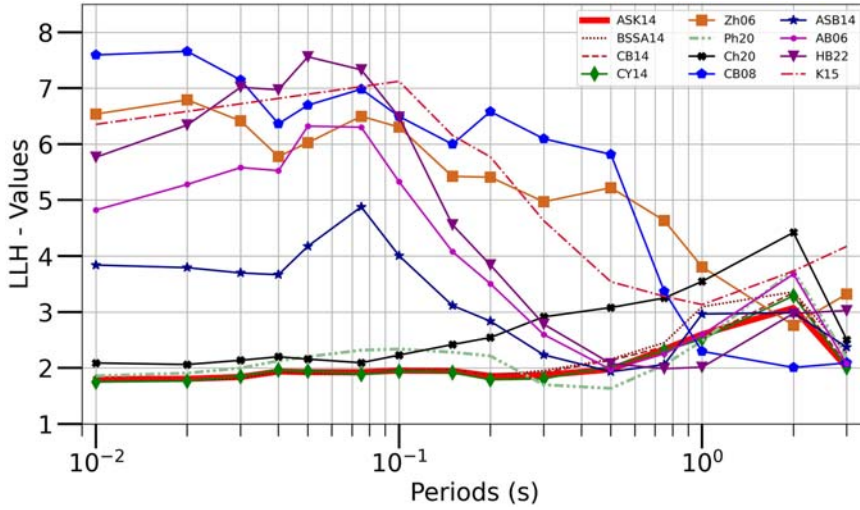


Figure 9. Plot log-likelihood (LLH) versus period for the selected candidate GMMs. This metric is used to evaluate the performance of the different GMMs relative to the observed ground motion data.

the Taiwanese models did. Given that the LLH and correlation values across all periods (Figure 8a and 8b) are relatively small, the NGA-West2 models generally perform good predictions with respect to the selected data. The NGA-West2 models can, therefore, be considered the most suitable foreign GMM for use in NVN; in this study, ASK14 was selected as a representative GMM to simulate seismic hazard scenarios of large earthquakes in NVN.

Figure 10 presents the residual analysis for between-event residual (δB_e), between-site residual ($\delta S2S_s$), and within-event and within-site residual (δWS_{es}) obtained from mixed effect regression (Bate et al., 2014) and plotted against magnitude (M), station ID, against distance (R_{HYP}) for ASK14 for periods of 0.01, 0.1, 0.2, and 1.0 s. The means and standard deviations were also computed and are presented in each subplot. The mean offset (mean residual) can be used to generally indicate overall model fit (all magnitudes and distance ranges). Specifically, the residuals at $T = 0.01, 0.1$, and 0.2 s with a mean near 0 indicate better fit than the residual at $T = 1.0$ s. However, the residuals are strongly dependent on magnitude at $T = 1.0$ s, indicating that ASK14 exhibits a stronger magnitude scaling than it is indicated by the data although the mean residual is near 0. In addition, the magnitude scaling of ASK14 (Figure 9) is unsuitable for long-period motion (1.0 s), for which it exhibits overprediction for $M5$ (by a factor of 1.5) and underprediction for $M3$ (by a factor of 1.5). The poor fit of the ASK14 model leads to high standard deviations for the long-period motion; the average acceptable standard deviation value for PSHA is approximately 0.8 (GeoPentech, 2015; Phung and Abrahamson, 2023). In this study, the estimated sigma (σ) values of the ASK14 predictions tested by the 2020 Moc-Chau earthquake recordings were 10% to 50% greater than the standard values for PSHA studies. Therefore, none of the GMMs considered in this study can be recommended for use in PSHA for NVN without further refinement. We recommend generating new GMMs with ASK14 as an initial model and modifying it as further events and observed data become available.

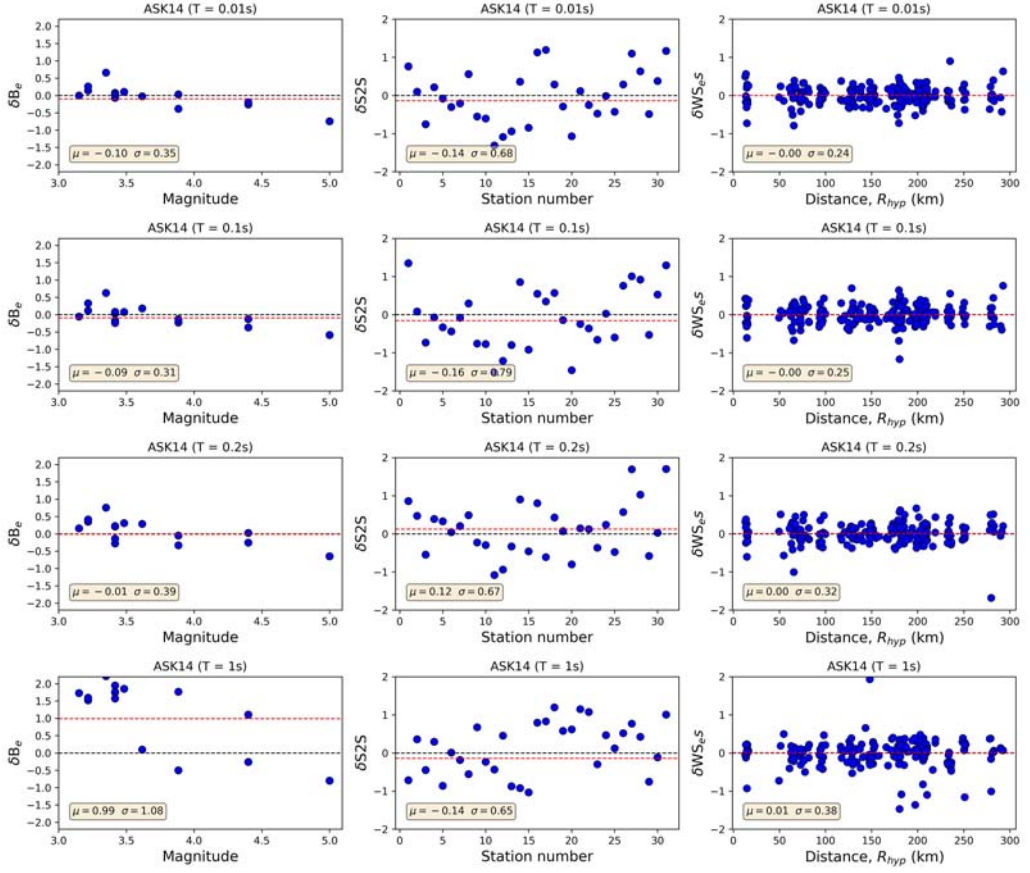


Figure 10. Residual analysis for ASK14 at $T = 0.01, 0.1, 0.2,$ and 1.0 s with data from the 2020 Moc-Chau earthquake sequence: between event residual (δB_e), between site residual ($\delta S2S$), and within-event and within-site residual plotted against magnitude (M), station ID, against distance (R_{hyp}). It is noted that the mean (μ [dashed line]) and standard deviation are also shown).

Adjustment of ASK14

The backbone model

For the purpose of predicting ground motion and evaluating seismic hazards due to the Moc-Chau earthquakes, we derive a backbone model that is an adjustment to ASK14 explicitly accounting for local effects in NVN. The methodology for deriving the backbone model is similar to that used in Sung et al. (2023) for France. Based on the peculiarities of the ground motion characteristics from the residuals, we identify two coefficients that control the ground motion in the considering earthquakes: coefficient a_6 measuring small magnitude scaling (the data available) and coefficient a_{17} representing distance attenuation. Basically, our method to modify ASK14 is to replace a_6 and a_{17} in ASK14 with new terms. Hence, the median prediction of ASK14 without small magnitude scaling and anelastic attenuation is

$$f_{ASK14-VN} = f_{ASK14} - (a_6(M - 5) + a_{17}R) \quad (5)$$

Table 4. List of the coefficients that determined the backbone model relative to ASK14.

Period (s)	a_6			a_{17}			Standard deviation	
	Estimate	Standard error	Origin	Estimate	Standard error	Origin	Estimate	Origin
0.01	1.64440	0.09582	2.15410	-0.01031	0.00128	-0.0072	0.6949	0.9329
0.02	1.63268	0.09660	2.14610	-0.01020	0.00133	-0.0073	0.7196	0.9637
0.03	1.62262	0.09850	2.15660	-0.01037	0.00136	-0.0075	0.7387	0.9950
0.05	1.61821	0.09679	2.08450	-0.01097	0.00140	-0.008	0.7777	1.0203
0.075	1.63958	0.10580	2.02850	-0.01159	0.00138	-0.0089	0.7492	0.9806
0.1	1.60627	0.10414	2.04080	-0.01172	0.00143	-0.0095	0.7903	1.0437
0.15	1.61975	0.11199	2.12080	-0.01039	0.00144	-0.0095	0.7554	1.1067
0.2	1.65092	0.08443	2.22410	-0.00962	0.00121	-0.0086	0.6577	1.0245
0.25	1.69069	0.09377	2.31240	-0.00862	0.00115	-0.0074	0.5924	0.9789
0.3	1.72682	0.09006	2.33830	-0.00729	0.00109	-0.0064	0.5467	0.9605
0.4	1.77359	0.10515	2.46880	-0.00561	0.00111	-0.0043	0.5016	0.9518
0.5	1.85902	0.13728	2.55860	-0.00429	0.00130	-0.0032	0.5125	1.0174
0.75	2.00184	0.18933	2.68210	-0.00189	0.00146	-0.0025	0.5263	1.2941
1	2.07575	0.21807	2.76300	-0.00088	0.00152	-0.0025	0.6187	1.5142
1.5	2.19005	0.23713	2.83550	0.00025	0.00134	-0.0022	0.7160	1.6673
2	2.10610	0.22641	2.89730	-0.00009	0.00089	-0.0019	0.7521	1.8327
3	1.93191	0.26668	2.90610	0.00000	0.00139	-0.0015	0.8229	2.2247

The term f_{ASK14} is the mean prediction from ASK14 given earthquake scenarios (M , R , etc.). Note that constant a_1 is not modified because we want to preserve the large magnitude scaling of the ASK14 in our backbone model. The mixed effect regression described in Bates et al. (2014) was applied in which the natural logarithm of spectral acceleration can be expressed as follows

$$\ln(y_{es}) = f_{ASK14-VN} + (a_{6vn}(M - 5) + a_{17vn}R) + \delta B_e + \delta S2S_s + \delta WS_{es} \quad (6)$$

where $\delta S2S_s$ and δWS_{es} are between site residual and within-event and within-site residual, respectively. Due to very limited data available for the regression, the aleatory total standard deviation of ASK14 is directly adopted without modification. Regressed coefficients (a_{6vn} and a_{17vn}) and related standard deviations are determined from the mixed effect regression. Table 4 lists the values of modified coefficients along with their standard errors. The original values are also included to emphasize the differences between the two models. Because of the limited data used in the regression, the standard error on the estimated coefficients is relatively large. The resulting model is less reliable when it predicts ground motion beyond the data used. Figure 11 shows the residual analysis with respect to magnitude (M), station ID, and distance; it indicates that residual trends of both δB_e in magnitude range and δWS_{es} in distance range are improved for the after-regression model (i.e., modified ASK14) as compared with that for the before-regression model. Obviously, the results indicate an improvement in the backbone model relative to ASK14.

On the other hand, Figure 12 displays a comparison of the magnitude scaling of the backbone and ASK14 for $R = 5, 10, 30$, and 70 km at $T = 0.01$ and 0.2 s. As expected, the results show the preservation of large-magnitude scaling of the backbone relative to the ASK14. With this improvement, the backbone can be used further for the hazard assessment. We generally modified two coefficients of ASK14 (a_6 and a_{17}) to improve the

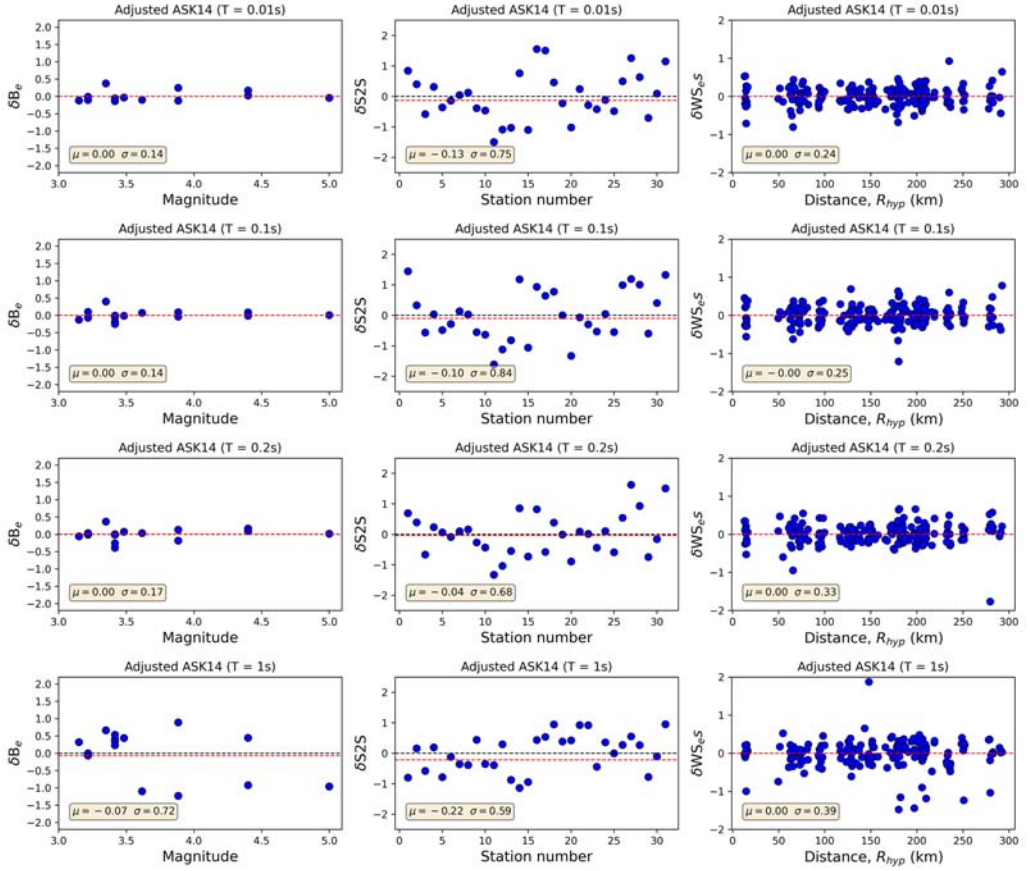


Figure 11. Residual analysis for the backbone model at $T = 0.01, 0.1, 0.2$, and 1.0 s with data from the 2020 Moc-Chau earthquake sequence: between-event residual (δB_e), between-site residual ($\delta S2S$), and within-event and within-site residual against magnitude (M), station ID, and distance (R_{hyp}). It is noted that the mean (μ [dashed line]) and standard deviation are also shown).

prediction of the Moc-Chau events. Eventually, we could choose to modify an additional coefficient a_2 , which controls the short-distance scaling; however, the resulting backbone would be less reliable for predicting the near-source distance because of the limited data used. Usually, the near-source component or the finite fault term of a GMM is constrained by simulations (Abrahamson et al., 2014). It can be determined from regression (Chiou and Youngs, 2014) if the observed data is well collected, covering a wide range of magnitude and short distance, such as the NGA-West2 data set.

The spatially varying coefficients model

In this section, the backbone model is adopted to derive the spatially varying coefficients model (VCM), which is conditioned on the earthquake's and station's coordinates. The VCM can be used to adjust the median response spectra to accurately predict ground motion for a scenario, which is similar to the approaches used for California and France (Lavrentiadis et al., 2021; Sung et al., 2022). According to the approaches, the adjustment

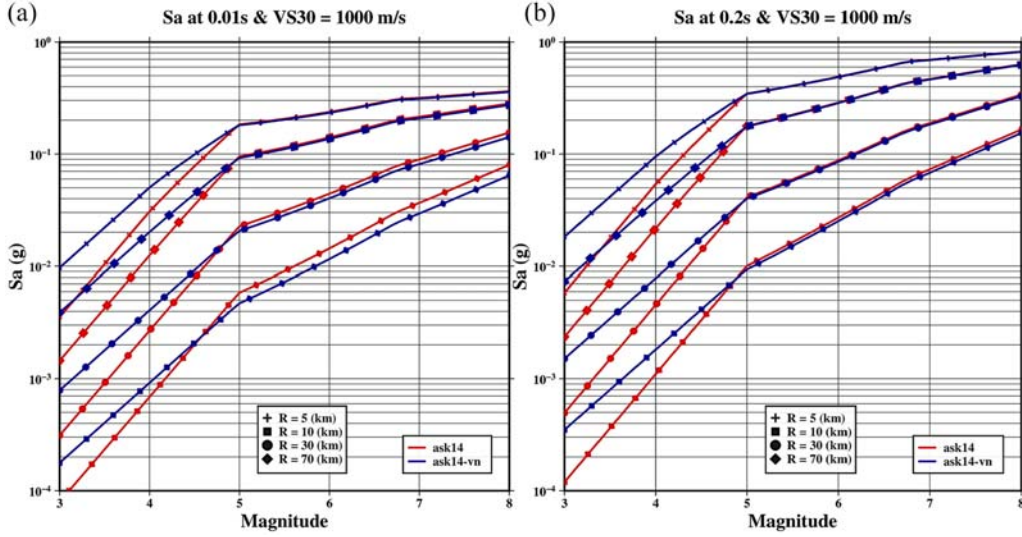


Figure 12. Comparison of magnitude scaling of ASK14 and its adjustment counterpart for SA at 0.01s (a) and SA at 0.2s (b) for distance = 5, 10, 30 and 70 km.

Note that the different distance scalings are labeled by curves with four different symbols.

terms also known as the spatially varying coefficients, which are defined later, can be derived using the following equation:

$$\ln(y_{es}) = [f_{erg}(M, R_{hyp}, V_{S30}) - c_{ca,erg} \cdot R_{hyp}] + \delta c_0 + \delta c_{1a,s}(t_s) + \delta c_{1b,s}(t_s) + \overrightarrow{c_{ca,P}}(t_c) \cdot \overrightarrow{\Delta R}(t_c) + \delta B_e + \delta W_{es} \quad (7)$$

where y_{es} is the ground motion intensity measure from e^{th} earthquake and s^{th} station. The term $f_{erg}(\dots)$ is the median prediction of the backbone model. The term $c_{cap,erg} \cdot R_{hyp}$ represents the anelastic attenuation of the backbone model, which is replaced by the cell-specific attenuation represented by the term $\overrightarrow{c_{ca,P}}(t_c) \cdot \overrightarrow{\Delta R}(t_c)$; $\overrightarrow{c_{ca,P}}(t_c)$ is a spatially varying anelastic attenuation coefficient as a function of the cell coordinate (t_c), and $\overrightarrow{\Delta R}(t_c)$ is a vector with all cell-path distance between earthquake e^{th} and station s^{th} , and $c_{cap,erg}$ is the anelastic attenuation coefficient of the backbone model. δc_0 is a constant shift; $\delta c_{1a,s}(t_s)$ is a spatially varying station adjustment as a function of the station coordinates (t_s); $\delta c_{1b,s}(t_s)$ is an independent site adjustment; δB_e is the between-event residuals; and δW_{es} is the within-event residual. These residuals have zero mean and standard deviation of τ and ϕ , respectively. Therefore, the total standard deviation of the derived model is computed as $\sigma_0 = \sqrt{\tau^2 + \phi^2}$. Note that the definition of notation described previously is followed by Lavrentiadis et al. (2022).

The spatially varying coefficients are modeled as a Gaussian process (GP) regression defined by a function $f(x)$ with zero mean and negative exponential covariance function (κ). We apply regression to the same regression model (Bayesian hierarchical model) and settings of the prior distribution similar to Lavrentiadis et al. (2021). The following equations are applied:

$$f(x) \sim GP(0, \kappa_{1,i}(t, t')) \quad (8)$$

$$\kappa_{1,i}(t, t') = \begin{cases} \omega_{1,as}^2 \cdot e^{-\frac{\|t_s - t'_s\|}{\ell_{1,as}}} & \text{for } i \in \{\delta c_{1as}\} \\ \omega_{1,bs}^2 \cdot \delta \|t_s - t'_s\| & \text{for } i \in \{\delta c_{1bs}\} \end{cases} \quad (9)$$

The calculation of the non-ergodic and elastic attenuation term is based on the methodology proposed by Dawood and Rodriguez-Marek, (2013) but modified to use the Bayesian formulation described by Kuehn et al. (2019). Non-overlapping, rectangular cells with a 20 x 20 km size are used to segment northern Vietnam. The spatially varying coefficient ($c_{ca,p}$) for cells is a multivariate normal distribution with an upper limit truncated to be less zero. The covariance function Eq. 9 consists of a negative exponential term and a diagonal term, which make anelastic attenuation have properties of continuous variation over a large area and independent variation from cell to cell.

$$c_{ca,p} \sim GP(c_{ca,erg}, \kappa_{ca,p}(t_c, t'_c)) \mathcal{L}(, 0) \quad (10)$$

$$\kappa_{1,i}(t, t') = \omega_{ca1,p}^2 \cdot e^{-\frac{\|t_c - t'_c\|}{\ell_{ca1,p}}} + \omega_{ca2,p}^2 \cdot \delta \|t_c - t'_c\| \quad (11)$$

The uncertainty of the spatially varying coefficient of mean prediction is computed using the following equation:

$$\Psi = K_i^* - k_i^T K_i^{-1} k_i \quad (12)$$

where K is the covariance between the spatially varying coefficients at the existing and existing locations ($K_i = k_i(t_s, t_s)$), k is the covariance between the spatially varying coefficients at the existing and new locations, and K^* is the covariance between the spatially varying coefficients at the new and new locations ($K^* = k_i(t_s^*, t_s^*)$). The parameters are estimated via Bayesian's inference using the program Stan (Stan Development Team, 2018). Hence, the results are the posterior distribution of the spatially varying coefficients, which captures their epistemic uncertainty and are shown in Figure 13 in terms of the site and path adjustment terms. Figure 13a and 13b show the spatially varying coefficient for the site term ($\delta c_{1as}(t_s)$) varying from -0.78 to 0.78 , where the larger values are given to the sites near the station recordings, and its absolute amplitude decreases and approaches zero for the sites quite far apart from the station recordings. Figure 13c and 13d show significant variation in the cell-specific attenuation coefficient values varying between -0.002 and -0.0254 in which the smaller values are given to the near-source region in the northwest-southeast direction, and the larger values are given to the far source region in the northwest-northeast direction. The range of the cell-specific attenuation coefficient values is smaller than that of ASK14, indicating a stronger distance attenuation of ground motion.

Figure 14 shows comparisons of distance attenuation of ASK14 with its adjustment counterpart for spectral acceleration at 0.01 s (or PGA) (Figure 14a) and 0.2 s (Figure 14b). These results show that the VCM presents a stronger distance attenuation than ASK14 for earthquakes with magnitudes of 4, 5, 6, and 7, which is consistent with the findings shown in Figure 13c and 13d. Taking the adjustment terms into account can change the median prediction for some locations significantly, depending on their values and the site's coordinates. Therefore, it is important to ensure that it makes sense and

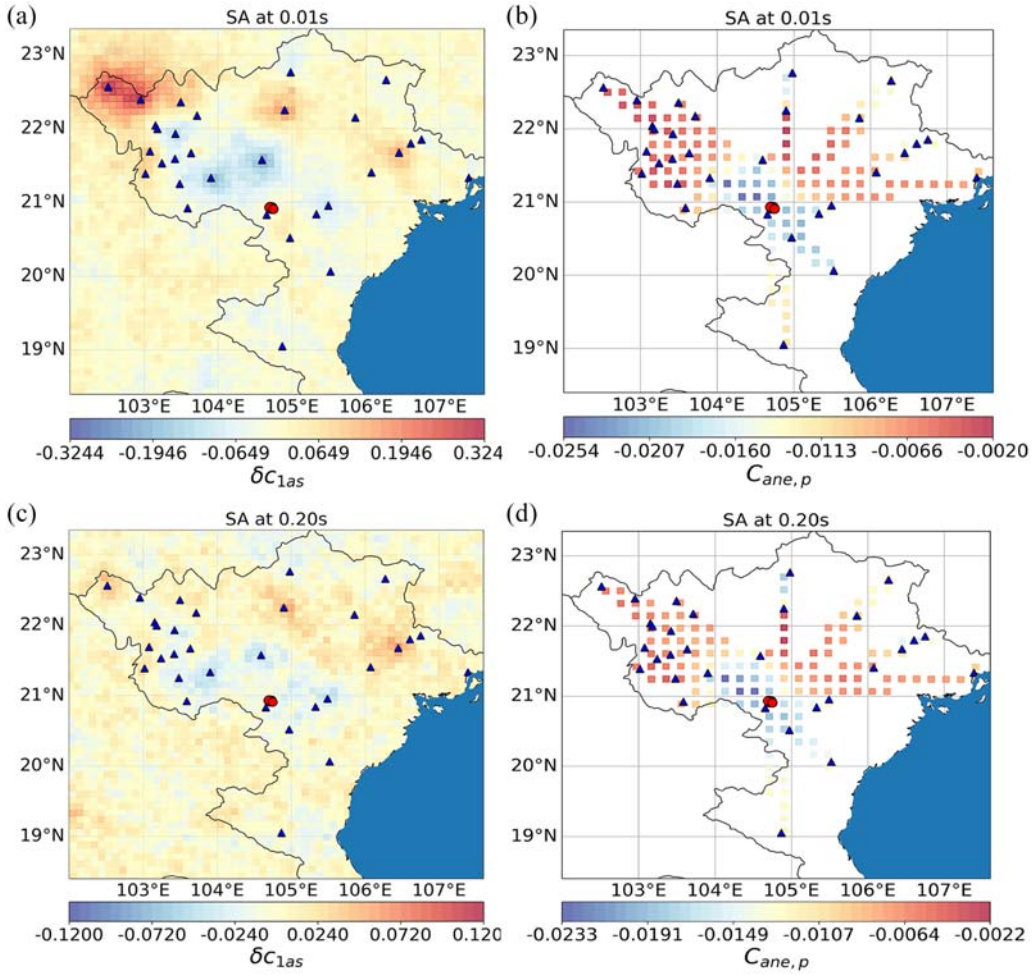


Figure 13. Map of the mean posterior distribution of the spatially varying coefficients (a, b) for site adjustment term and (c, d) for cell-specific attenuation adjustment term for PGA and SA at 0.2 s. The Moc-Chau earthquake epicenter (red dot) and 31 recorded stations (triangles) are also plotted. A representative site (rectangular) is located on a thick deposit alluvial area of the capital, Hanoi city.

leads to an improvement of the resulting model. As a check, the residuals (between-event residual, between-site residual, and within-event and within-site residual) of the backbone model and the VCM are plotted against magnitude (M), station number, and hypo-center distance (R_{hyp}) in Figure 15.

Seismic hazard assessments for large earthquake scenarios

To assess seismic hazards in Vietnam, given a ground acceleration level for each zone, the design spectra can be computed according to the seismic design code TCVN 9386:2012 (Appendix A). Figure 16 presents the design spectra for ground types A, B, C, D, and E in Hanoi with $a_g = 0.04$ g. In Figure 16, the computed spectral accelerations of the seismograms recorded at station MCVB (12.4 km away from the epicenter) during the 2020

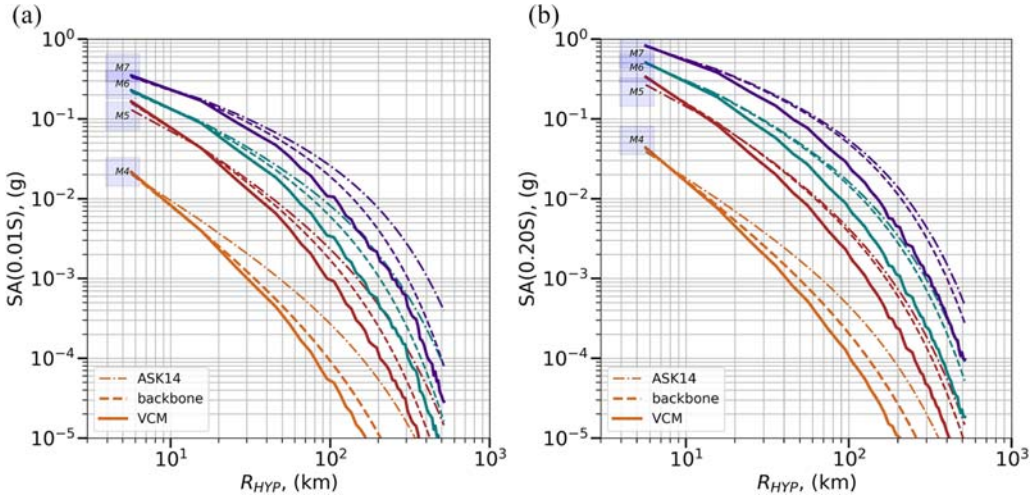


Figure 14. Comparison of distance scaling of VCM (solid curves) with those of the backbone (dashed-curves) and ASK14 (dashed -dotted curve) for SA at 0.01s (a) and SA at 0.2s (b) for $M = 4, 5, 6$, and 7 .

Moc-Chau earthquake sequence were superimposed with the design spectra of TCVN 9386:2012 for comparison. The acceleration spectra of the mainshock ($M_W = 5.0$) exceeded the TCVN 9386:2012 design spectra at periods of approximately 0.03 to 0.1 s; the maximum site amplifications (i.e., group D and E in Figure 16) were included for a conservative comparison. This implies that a similar earthquake ($M_W = 5$) occurred approximately 10 to 15 km away from Hanoi City, which may have damaged buildings and infrastructure. However, the distance from the earthquake source to Hanoi is more than 120 km; at this distance, the observed acceleration response spectra from other stations at similar distances did not exceed the design spectra, which implies that the earthquakes could not have damaged buildings in the Hanoi area. However, previous seismic hazard assessments have suggested that a giant super-shear rupture destructive earthquake may occur along the Red River fault (Das, 2015; Duan et al., 2013; Robinson et al., 2010). A larger earthquake occurring along the fault will likely greatly damage buildings in Hanoi City, and engineers and policymakers must not ignore this possibility.

Actually, the explicit accounts for the regional path effects of a global GMM may reduce its variation further. In this study, we use the data from Moc-Chau events to provide an adjustment to ASK14 that explicitly accounts for the regional path effects in NVN by introducing the spatially varying coefficients through this new data. The modification followed a method similar to that used in Kuehn et al. (2019). The predictions from the backbone model generally align well with the observed ground motions, demonstrating the value of incorporating new observations to improve regional ground motion predictions using an existing GMM. It is noted that the adjustment of ASK14 in this analysis was based on relatively few events and records, with particular source properties and particular propagation path effects. The analysis will produce a different observation because attenuation may change for an occurrence on a different fault at a different depth and for a different fault mechanism.

One of the applications of GMMs is to use both the backbone and VCM to predict large earthquake scenarios providing a platform for evaluating seismic hazards. The

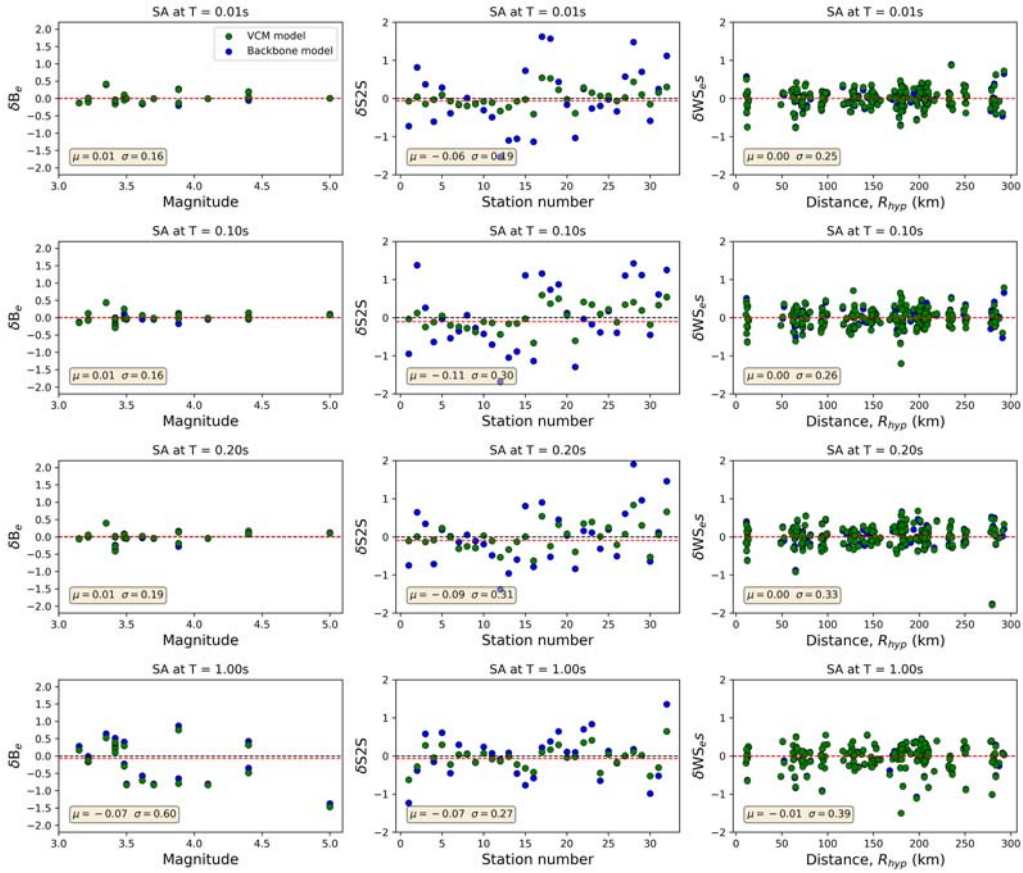


Figure 15. Comparison of VCM's residuals with the backbone model at $T = 0.01, 0.1, 0.2$, and 1.0 s with data from the 2020 Moc-Chau earthquake sequence: between-event residual (δB_e), between-site residual ($\delta S2S$), and within-event and within-site residual against magnitude (M), station ID, and distance (R_{hyp}). It is noted that the mean (μ [dashed line]) and standard deviation are also shown).

GMM predictions are then used to explore the possibility of damage caused to buildings and infrastructure in Hanoi if a large earthquake ($M_s 6.8 \sim$ the highest historical earthquake magnitude) occurred at the closest fault of about 80 to 150 km away from Hanoi City and as an example of events near the 2020 Moc-Chau earthquake epicenter (i.e., in the Ma river fracture zone [Wen et al., 2015, and Wu et al., 2018]). A representative site of Hanoi City is located on the thick deposit of dense alluvium soils with v_s of 200 m/s as a representative site (Figure 17a). We estimate the response spectrum at a representative site selected for the construction of the typical rigid structures with a period of 0.2 s. The engineers leading the design of the structure are concerned about the seismic demands during an earthquake of similar magnitude and with a predominant period close to the structure's resonant period. We conduct a deterministic seismic hazard assessment to estimate the seismic demand at the foundation level of the structure. A deterministic scenario is defined based on the site's characteristics and the response spectrum estimated using the VCM (Figure 17a). For practical purposes, this spectrum is considered representative of the seismic demand at the base of the alluvial deposit. For the case in which the backbone and

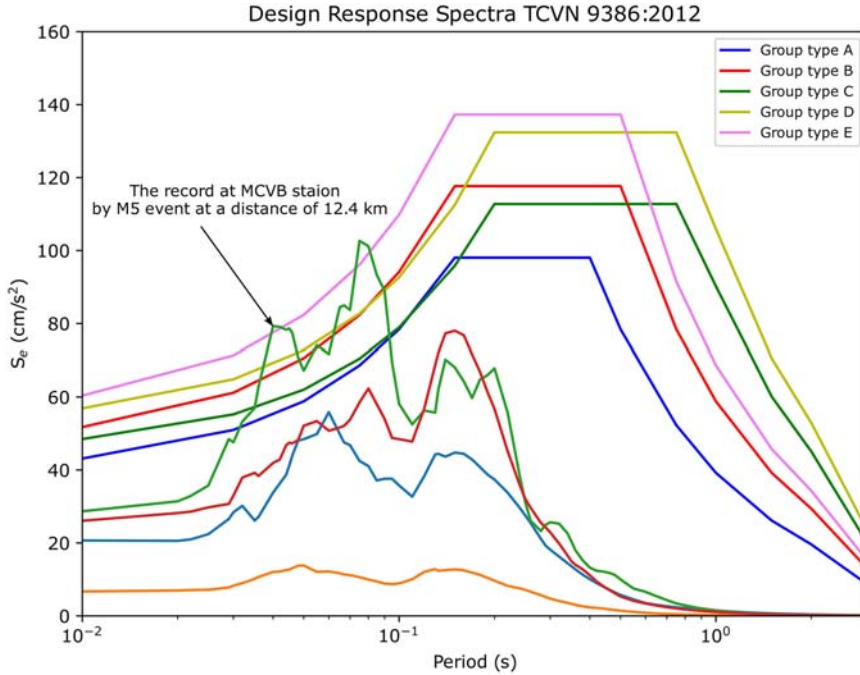


Figure 16. Superposition of the acceleration spectra (mainshock and three aftershocks with magnitude 4.4, 4.1, and 3.4, respectively) from station MCVB and the design spectra. The design ground acceleration (a_g) of 0.04 g was used to generate this plot according to the ground acceleration zone map of Figure B1(b) (Supplementary Appendix B).

VCM model is used with $M = 6.8$ (Figure 17b), the shaded area represents the lower bound (-1σ) and upper bound ($+1\sigma$) around the median predictions calculated for $R = 120$ km, which is the influence range on the structure damage. Both predicted spectral acceleration values of the backbone and VCM are compared with the TCVN 9386:2012 design spectra. It shows that the predicted ground motions exceed the design values in a wide period range, especially on the periods $T > 0.3$ s. It should be noted that according to the proposed design spectra and the variability of observed ground motions, the range of the structure damage from an M6.8 event could be more severe than that considering the median prediction from the VCM. This requires further analyses of the ground motion characteristics observed at these stations for seismic hazard assessment.

Discussion and conclusion

In this study, the 2020 Moc-Chau earthquake sequence with 13 events was used to evaluate the performance of the selected GMMs. For this analysis, V_S^{30} is a site parameter used in most selected GMMs, and errors in V_{S30} estimations can have a direct impact on the variability of selected GMMs. We demonstrated that the predominant period (T_g), as determined by the average HVSF for each site, is an effective approximation for V_S^{30} in NVN. Through the analysis, the site response model of selected GMMs can generally correlate well with the estimated V_S^{30} . However, the applicability of the T_g from CENA region as a V_S^{30} proxy to NVN may contain large uncertainty and bias because the geological site

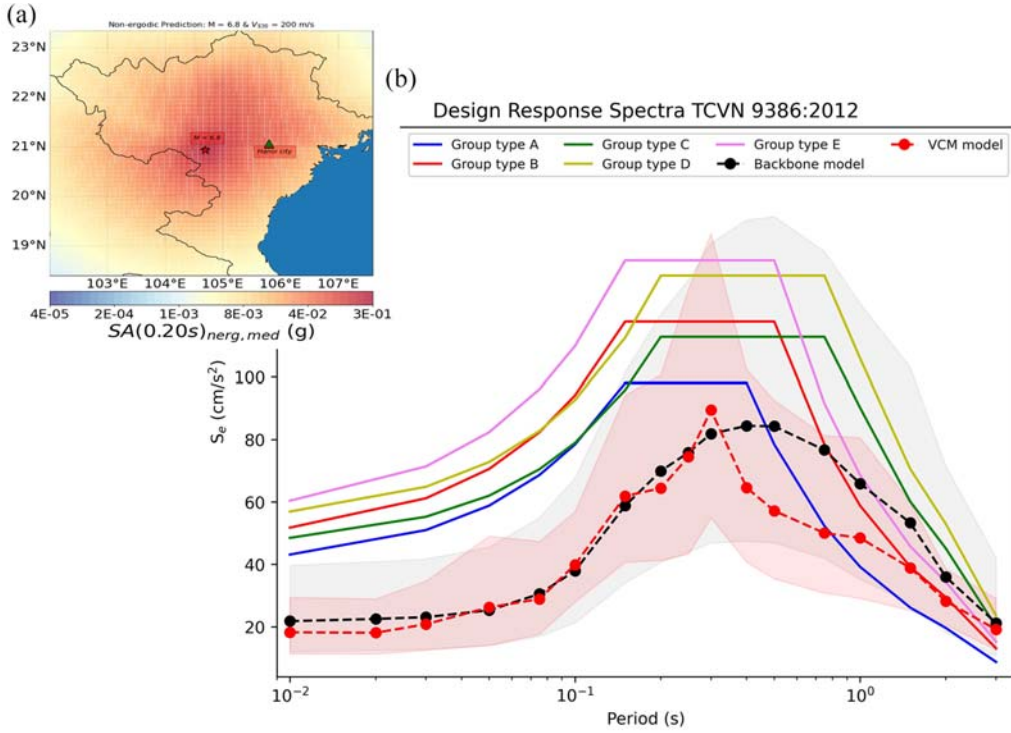


Figure 17. (a) A map of $S_a(0.2\text{ s})$ predicted by a VCM model for a hypothetical magnitude (M) of 6.8 occurred at Moc-Chau, and a considered site at Hanoi City is located about 120–130 km away from the epicenter. (b) Superposition of a hypothetical earthquake $M6.8$ predicted the backbone (black dots) and VCM model (red dots) at the representative site and the design spectra. The shaded area represents the median ± 1 standard deviation.

condition is different from region to region. In case of a lack of V_S^{30} information, we temporarily accept such a limitation, and the estimated V_S^{30} will be verified once the measurement V_S^{30} is available.

The log-likelihood (LLH) analysis, as the quick assessment, showed that the NGA-West2 GMMs (4 out of 12 GMMs) fit the observed data better than other models did. The global ASK14, one of the NGA-West2 GMMs, was selected for the residual analysis to better understand which GMM components respond differently to the observed data. The small magnitude scaling and distance attenuation of ASK14 are not supported by the observed data. For the seismic hazard reduction in NVN, an ad hoc GMM must be developed or adjusted to accurately predict ground motion. Since the data is limited (only $M < 5.0$), adjusting a global GMM is preferred rather than developing a new model. As an example of the GMM adjustment, the backbone model resulted from modifying ASK14 in the small magnitude scaling and anelastic attenuation term. The spatially varying coefficients model was then developed by incorporating the event and the station's coordinates into the backbone model. However, the applicability of these models is limited due to the limited available earthquake sources or a small number of recorded events. In this study, the adjusted models can only be used for the purpose of investigating the ground motion characteristic of the Moc-Chau earthquakes. For the development of the PSHA study for

the NVN or other engineering applications, a new GMM needs to be developed by using the additional ground motion data at stations from future earthquakes.

According to the complementary evaluations of this study, local observations are required to develop this region-specific GMM. However, in the NVN, only limited local strong-motion data have been recorded because of its sparse station distribution and low seismicity. The available data are insufficient for the development of a representative GMM for NVN. Fortunately, as indicated by this study (Figure 3) and others (Edwards et al., 2021; Novakovic et al., 2018), the velocity seismograms from the broadband sensors support earthquake engineering applications. The continuous recording system of the broadband seismic network may contribute to the collection of more data than that collected from independent trigger-mode strong-motion stations; therefore, the required input data for GMM development can be collected from the VN seismic network in the near future.

Furthermore, seismic records from a 25-station broadband network designed for tectonic and crust structure studies in the NVN (deployed by the Institute of Earth Sciences of Academia Sinica, Taiwan, continuously from 2005) may also be used to collect data for GMM development (Huang et al., 2009). Nevertheless, records of ground motion from large-magnitude or near-source events from such broadband velocity sensors may be over-scaled and may exhibit waveform distortion, which limits their applicability. However, after the available data were examined, such distortions were limited in the existing broadband records for NVN. By combining the existing broadband velocity data (Huang et al., 2009) and the possible new collecting data from the VN seismic network, one can extend the database for developing local GMM, thereby benefitting the seismic hazard assessments and seismic design planning for high-rise buildings, nuclear power plants, hydraulic dams, large industrial factories, and public facilities in Vietnam.

The 2020 Moc-Chau earthquake ($M_w = 5$) and its aftershocks elucidated several aspects of ground motion characteristics and their effects on structural damage. Based on the comparison of the computed response spectra of the records and the design spectra, our examination of the seismic hazard scenarios of large earthquakes in NVN indicated the possibility of damage resulting from shaking in the Hanoi metropolitan area with current design codes caused by earthquake sources in NVN. Furthermore, the vertical ground motion observed at the MCVB station being greater than the GM of its horizontal components should be carefully considered in the seismic design of near-source structures because the effects of vertical motion are often neglected by engineers. A further evaluation similar to this study is suggested to be conducted using a set of vertical GMMs for near-source regions. We suggest developing a new GMM in the near future based on additional input data collected from existing broadband seismic records and the new Vietnam broadband seismic network. A careful integration of the old and new seismic data will improve the accuracy of seismic hazard assessment in Vietnam.

Acknowledgments

We appreciate the staff of the Vietnam Academy of Science and Technology and Academia Sinica for collecting the data used in this study, and we are especially grateful to Prof. Norman Abrahamson for his guidance and thoughtful comments. We thank Dr. Karen Sung for providing help in implementing the non-ergodic regression method. We are grateful for Prof. Editor Jack Baker's and reviewer's remarks, which helped to strengthen our work and increase its value.


Declaration of conflicting interests


The author(s) declared no potential conflicts of interest with respect to the research, authorship, and/or publication of this article.


Funding


The author(s) disclosed receipt of the following financial support for the research, authorship, and/or publication of this article: This study has been funded by Vietnam Academy of Science and Technology (VAST) under grant numbers VAST06.02/23-24 and VAST05.02/23-24 and Ministry of Science and Technology of Vietnam under the grant number TLCN.58/22, and by Taiwan's Ministry of Science and Technology under grants MOST 108-2116-M-001-011, MOST 108-2116-M-001-010-MY3, and MOST 109-2119-M-001-011.

ORCID iDs

Van-Bang Phung  <https://orcid.org/0000-0002-3269-7792>

Cong Nghia Nguyen  <https://orcid.org/0000-0003-2740-602X>

Grigorios Lavrentiadis  <https://orcid.org/0000-0001-6546-1340>

Chung-Han Chan  <https://orcid.org/0000-0003-1875-3652>

Data and resources

Ground motion data for this study are provided by the Vietnam National Network at the Vietnam Academy of Science and Technology and the Institute of Earth Sciences, Academia Sinica. The code and data of this study are available on Phung et al. (2024). The regression method for this study was performed using STAN and cmdstan as it is implemented in ngmm_tools (https://github.com/NHR3-UCLA/ngmm_tools). The MATLAB code for implementing the GMMs was downloaded from the Baker research group (https://www.jackwbaker.com/GMMs_archive.html).

Supplemental material

Supplemental material for this article is available online.

References

- Abrahamson N A, Silva WJ and Kamai R (2014) Summary of the ASK14 ground motion relation for active crustal regions. *Earthquake Spectra* 30(3): 1025–1055. <https://doi.org/10.1193/070913EQS198M>.
- Akkar S, Sandikkaya MA and Bommer JJ (2014) Empirical ground-motion models for point- and extended-source crustal earthquake scenarios in Europe and the Middle East. *Bulletin of Earthquake Engineering* 12(1): 359–387. <https://doi.org/10.1007/s10518-013-9461-4>.
- Atkinson GM and Boore DM (2006) Earthquake ground-motion prediction equations for eastern North America. *Bulletin of the Seismological Society of America* 96(6): Article 6.
- Bommer JJ (2012) Challenges of building logic trees for probabilistic seismic hazard analysis. *Earthquake Spectra* 28(4): 1723–1735. <https://doi.org/10.1193/1.4000079>.
- Bommer JJ, Douglas J, Scherbaum F, Cotton F, Bungum H and Fäh D (2010) On the selection of ground-motion prediction equations for seismic hazard analysis. *Seismological Research Letters* 81(5): Article 5. <https://doi.org/10.1785/gssrl.81.5.783>.
- Bommer JJ, Scherbaum F, Bungum H, Cotton F, Sabetta F and Abrahamson NA (2005) On the use of logic trees for ground-motion prediction equations in seismic-hazard analysis. *Bulletin of the Seismological Society of America* 95(2): 377–389.

- Boore DM, Stewart JP, Seyhan E and Atkinson GM (2014) NGA-West2 equations for predicting PGA, PGV, and 5% damped PSA for shallow crustal earthquakes. *Earthquake Spectra* 30(3): 1057–1085. <https://doi.org/10.1193/070113EQS184M>.
- Bozorgnia Y, Abrahamson NA, Atik LA, Ancheta TD, Atkinson GM, Baker JW, Baltay A, Boore DM, Campbell KW, Chiou BS-J, Darragh R, Day S, Donahue J, Graves RW, Gregor N, Hanks T, Idriss IM, Kamai R, Kishida T and ... Youngs R (2014) NGA-West2 research project. *Earthquake Spectra* 30(3): 973–987. <https://doi.org/10.1193/072113EQS209M>.
- Bozorgnia Y and Campbell KW (2016) Ground motion model for the vertical-to-horizontal (v/h) ratios of PGA, PGV, and response spectra. *Earthquake Spectra* 32(2): 951–978. <https://doi.org/10.1193/100614EQS151M>.
- Campbell KW and Bozorgnia Y (2008) NGA ground motion model for the geometric mean horizontal component of PGA, PGV, PGD and 5% damped linear elastic response spectra for periods ranging from 0.01 to 10 s. *Earthquake Spectra* 24(1): 139–171. <https://doi.org/10.1193/1.2857546>.
- Campbell KW and Bozorgnia Y (2014) NGA-West2 ground motion model for the average horizontal components of PGA, PGV, and 5% damped linear acceleration response spectra. *Earthquake Spectra* 30(3): 1087–1115. <https://doi.org/10.1193/062913EQS175M>.
- Chao SH, Chiou BS-J, Hsu CC and Lin PS (2019) A horizontal ground-motion model for crustal and subduction earthquakes in Taiwan. *Earthquake Spectra* 36(2): 463–506. <https://doi.org/10.1177/8755293019891711>.
- Chiou BS-J and Youngs RR (2014) Update of the Chiou and Youngs NGA model for the average horizontal component of peak ground motion and response spectra. *Earthquake Spectra* 30(3): 1117–1153. <https://doi.org/10.1193/072813EQS219M>.
- Das S (2015) Supershear earthquake ruptures—theory, methods, laboratory experiments and fault superhighways: an update. In: *Perspectives on European Earthquake Engineering and Seismology*. Springer, Cham: 1–20.
- Dawood HM and Rodriguez-Marek A (2013) A method for including path effects in ground-motion prediction equations: an example using the Mw 9.0 Tohoku earthquake aftershocks. *Bulletin of the Seismological Society of America* 103(2B): 1360–1372. <https://doi.org/10.1785/0120120125>.
- Di Alessandro C, Bonilla LF, Boore DM, Rovelli A and Scotti O (2012) Predominant-period site classification for response spectra prediction equations in Italy. *Bulletin of the Seismological Society of America* 102(2): 680–695. <https://doi.org/10.1785/0120110084>.
- Duan BV, Thang NC, Vuong NV and Nguyen PD (2013) The magnitude of the largest possible earthquake in the Muong La-Bac Yen fault zone. *Vietnam Journal of Earth Sciences* 35(1): Article 1.
- Duong NA, Sagiya T, Kimata F, To TD, Hai VQ, Cong DC, Binh NX and Xuyen ND (2013) Contemporary horizontal crustal movement estimation for northwestern Vietnam inferred from repeated GPS measurements. *Earth Planets and Space* 65(12): Article 12. <https://doi.org/10.5047/eps.2013.09.010>.
- Edwards B, Crowley H, Pinho R and Bommer JJ (2021) Seismic hazard and risk due to induced earthquakes at a shale gas site. *Bulletin of the Seismological Society of America* 111 (2): 875–897. <https://doi.org/10.1785/0120200234>.
- Emolo A, Sharma N, Festa G, Zollo A, Convertito V, Park J, Chi H and Lim I (2015) Ground-motion prediction equations for South Korea Peninsula. *Bulletin of the Seismological Society of America* 105(5): 2625–2640. <https://doi.org/10.1785/0120140296>.
- GeoPentech (2015) Southwestern United States Ground Motion Characterization SSHAC Level 3 – Technical Report Rev.2.
- Hassani B and Atkinson GM (2016a) Site-effects model for Central and Eastern North America Based on peak frequency. *Bulletin of the Seismological Society of America* 106(5): 2197–2213. <https://doi.org/10.1785/0120160049>.
- Hassani B and Atkinson GM (2016b). Applicability of the site fundamental frequency as a VS 30 proxy for central and eastern North America. *Bulletin of the Seismological Society of America*, 106(2): 653–664

- Huang BS, Le TS, Liu CC, Toan DV, Huang WG, Wu YM, Chen YG and Chang WY (2009) Portable broadband seismic network in Vietnam for investigating tectonic deformation, the Earth's interior, and early-warning systems for earthquakes and tsunamis. *Journal of Asian Earth Sciences* 36(1): Article 1. <https://doi.org/10.1016/j.jseaes.2009.02.012>.
- Kuehn NM, Abrahamson NA and Walling MA (2019) Incorporating nonergodic path effects into the NGA-West2 ground-motion prediction equations. *Bulletin of the Seismological Society of America* 109(2): 575–585. <https://doi.org/10.1785/0120180260>.
- Lap NK (1991) The seismotectonics of the Indochina peninsula. *Journal of Southeast Asian Earth Sciences* 6(2): Article 2.
- Lavrentiadis G, Abrahamson NA and Kuehn NM (2023) A non-ergodic effective amplitude ground-motion model for California. *Bulletin of Earthquake Engineering* 21(11): 5233–5264. <https://doi.org/10.1007/s10518-021-01206-w>.
- Lavrentiadis G, Abrahamson NA, Nicolas KM, Bozorgnia Y, Goulet CA, Babič A, Macedo J, Dolšek M, Gregor N, Kottke AR, Lacour M, Liu C, Meng X, Phung V-B, Sung C-H and Walling M (2023) Overview and introduction to development of non-ergodic earthquake ground-motion models. *Bulletin of Earthquake Engineering* 21(11): 5121–5150. <https://doi.org/10.1007/s10518-022-01485-x>.
- Lu NT, Burmin VY, Hang PTT, Hoan VT and Giang HT (2018) Estimation of errors in determination of main parameters of earthquake hypocenter, recorded by the national seismic network of Vietnam. *Vietnam Journal of Earth Sciences* 40(1): Article 1. <https://doi.org/10.15625/0866-7187/40/1/10875>.
- Lu NT, Rodkin MV, Phuong TV, Hang PTT, Quang N and Hoan VT (2016) Algorithm and program for earthquake prediction based on the geological, geophysical, geomorphological and seismic data. *Vietnam Journal of Earth Sciences* 38(3): Article 3.
- Medvedev SV and Sponheuer W (1969) Scale of seismic intensity. In *Proc. IV World Conference of the Earthquake Engineering*, Santiago, Chile. A-2: 143–153.
- Mercado V, Pajaro CA, Arteta CA, Diaz FJ, Montejo J, Arcila M and Abrahamson NA (2023) Semiempirical model for the estimation of site amplification in Northern South America. *Earthquake Spectra* 39(2): 1109–1139. <https://doi.org/10.1177/87552930231153190>.
- Nakamura Y (1989) A Method for Dynamic Characteristics Estimation of Subsurface Using Microtremor on the Ground Surface. *Railway Technical Research Institute, Quarterly Reports*, 30(1). <https://trid.trb.org/View/294184>.
- NCREE (2015) Reevaluation of probabilistic seismic hazard of nuclear facilities in Taiwan using SSHAC level 3 methodology project. Available at: [Http://sshac.ncree.org.tw](http://sshac.ncree.org.tw) (accessed 31 December 2019). National Center for Research on Earthquake Engineering (NCREE).
- Nguyen CN, Nguyen VD, Ha TG, Dinh QV, Nguyen LM, Huang BS, Pham TT, Nguyen HT, Le QK and Nguyen HH (2022) Automatic earthquake detection and phase picking in Muong Te, Lai Chau region: An application of machine learning in observational seismology in Vietnam. *Vietnam Journal of Earth Sciences*: 430–446. <https://doi.org/10.15625/2615-9783/17253>.
- Nguyen CN, Nguyen VD, Nguyen LM, Phung VB, Huang B-S, Nguyen AD, Le QK, Giang HT, Dinh QV, Ha VL and Chen PF (2022a) Characteristics of earthquake source and ground motions in Northern Vietnam investigated through the 2020 Moc Chau M5.0 earthquake sequence. *Journal of Asian Earth Sciences* 229: 105–144. <https://doi.org/10.1016/j.jseaes.2022.105144>.
- Nguyen DX (2005) *Research and Forecasting Earthquakes and Ground Movements in Vietnam*. Hanoi, Vietnam: Vietnam Institute of Geophysics (in Vietnamese).
- Nguyen DX and Le TS (2005) Seismic hazard assessment for Vietnam Territory. In: *Proceedings of the 4th Conference of Vietnamese Association of Geophysics Hanoi*, Vietnam Publishing House of Science and Technology, pp. 281–304.
- Nguyen HP, Pham TT and Nguyen TN (2019) Investigation of long-term and short-term seismicity in Vietnam. *Journal of Seismology* 23(5): Article 5. <https://doi.org/10.1007/s10950-019-09846-x>.
- Nguyen LM, Lin TL, Wu YM, Huang BS, Chang CH, Huang WG, Le TS, Nguyen QC and Dinh VT (2012) The first peak ground motion attenuation relationships for North of Vietnam. *Journal of Asian Earth Sciences*, 241–253. <https://doi.org/10.1016/j.jseaes.2011.09.012>.

- Nguyen VQ, Aaqib M, Nguyen DD, Luat NV and Park D (2020) A site-specific response analysis: A case study in Hanoi, Vietnam. *Applied Sciences* 10(11): Article 11.
- Nizamani ZA and Park D (2021) Testing Ground-Motion Prediction Equations against Moderate Magnitude Earthquake Data Recorded in Korea. *Bulletin of the Seismological Society of America* 111(1): 321–338. <https://doi.org/10.1785/0120200095>.
- Novakovic M, Atkinson GM and Assatourians K (2018) Empirically calibrated ground-motion prediction equation for Oklahoma. *Bulletin of the Seismological Society of America* 108(5A): Article 5A.
- Ornthammarath T, Warnitchai P, Chan CH, Wang Y, Shi X, Nguyen PH, Nguyen LM, Kosuwan S and Thant M (2020) Probabilistic seismic hazard assessments for Northern Southeast Asia (Indochina): Smooth seismicity approach. *Earthquake Spectra* 36 (1_suppl), 69–90. <https://doi.org/10.1177/8755293020942528>.
- Pailoplee S and Choowong M (2014) Earthquake frequency-magnitude distribution and fractal dimension in mainland Southeast Asia. *Earth Planets and Space* 66(1): Article 1. <https://doi.org/Art810.1186/1880-5981-66-8>.
- PEER (2015) *NGA-East: Median ground-motion models for the central and eastern North America region*. PEER Report No. 2015/04. Berkeley, CA: Pacific Earthquake Engineering Research Center, University of California.
- Pham TT and Nguyen HP (2019) Probabilistic Seismic Hazard Assessment for Hanoi City. *Vietnam Journal of Earth Sciences* 41(4): 321–338. <https://doi.org/Doi:10.15625/0866-7187/41/4/14235>.
- Phung VB and Abrahamson NA (2023) Conditional ground-motion model based on RVT spectral moments for converting Fourier amplitude spectra to response spectra. *Bulletin of Earthquake Engineering* 21(11): 5175–5207. <https://doi.org/10.1007/s10518-022-01559-w>.
- Phung VB, Abrahamson NA, Huang BS and Loh CH (2022) Vertical ground-motion prediction equation and the vertical-to-horizontal spectral ratio for crustal earthquakes in Taiwan. *Earthquake Spectra* 38(2): 1189–1222. <https://doi.org/10.1177/87552930211061168>.
- Phung VB, Loh CH, Chao SH and Abrahamson NA (2018) Analysis of epistemic uncertainty associated with GMPEs and their weight within the logic tree for PSHA: Application to Taiwan. *Terr. Atmos. Ocean. Sci.* 29: 611–633. <https://doi.org/doi:10.3319/TAO.2018.08.13.01>
- Phung VB, Loh CH, Chao SH and Chiou BSJ (2020) Ground motion prediction equation for crustal earthquakes in Taiwan. *Earthquake Spectra* 36(4): 2129–2164. <https://doi.org/10.1177/8755293020919415>.
- Phung VB, Nguyen C.N and Ha VL (2024) Program code and data for paper “Evaluation of Ground Motion Models for Northern Vietnam based on Ground Motion Records of the 2020 Moc-Chau Mw5.0 earthquake sequence.” Zenodo. <https://doi.org/10.5281/zenodo.10525914>.
- Phuong NH (1991) Probabilistic assessment of earthquake hazard in Vietnam based on seismotectonic regionalization. *Tectonophysics* 198(1): Article 1.
- Robinson DP, Das S and Searle MP (2010) Earthquake fault superhighways. *Tectonophysics* 493(3–4): Article 3–4. <https://doi.org/10.1016/j.tecto.2010.01.010>.
- Scherbaum F, Delavaud E and Riggelsen C (2009) Model selection in seismic hazard analysis: An information-theoretic perspective. *Bulletin of the Seismological Society of America* 99(6): 3234–3247.
- Stan Development Team (2018) CmdStan: The command-line interface to Stan, Version 2.18.0. Available at: <http://mc-stan.org> (last accessed December 2018).
- Sung CH, Abrahamson NA, Kuehn NM, Traversa P and Zentner I (2023) A non-ergodic ground-motion model of Fourier amplitude spectra for France. *Bulletin of Earthquake Engineering* 21(11): 5293–5317. <https://doi.org/10.1007/s10518-022-01403-1>.
- Tapponnier P, Peltzer G, Ledain AY, Armijo R and Cobbold P (1982) Propagating extrusion tectonics in Asia—new insights from simple experiments with plasticine. *Geology* 10(12): Article 12. [https://doi.org/Doi10.1130/0091-7613\(1982\)10<611:Petian>2.0.Co;2](https://doi.org/Doi10.1130/0091-7613(1982)10<611:Petian>2.0.Co;2).
- Tran VH and Kiyomiya O (2012) Ground motion attenuation relationship for shallow strike-slip earthquakes in Northern Vietnam Based on Strong motion records from Japan, Vietnam and adjacent regions. *Journal of Japan Society of Civil Engineers, Ser. A1 (Structural Engineering & Earthquake Engineering (SE/EE))* 29: 23s–39s. <https://doi.org/10.2208/jscseee.29.23s>.

- Tran VH and Kiyomiya O (2013) Source parameter estimation and stochastic ground motion simulation based on recorded accelerograms in Northwestern Vietnam. *Journal of Earthquake Engineering* 17(3): Article 3. <https://doi.org/10.1080/13632469.2012.719484>.
- Tuyen NH and Lu NT (2012) Recognition of earthquake-prone nodes, a case study for North Vietnam ($M \geq 5.0$). *Geodesy and Geodynamics* 3(2): Article 2.
- Wald DJ, Quitoriano V, Worden CB, Hopper M and Dewey JW (2012) USGS “Did You Feel It?” internet-based macroseismic intensity maps. *Annals of Geophysics* 54(6): Article 6.
- Wen S, Yeh YL, Tang CC, Phong LH, Toan DV, Chang WY and Chen CH (2015) The tectonic structure of the Song Ma fault zone, Vietnam. *Journal of Asian Earth Sciences* 107: 26–34. <https://doi.org/10.1016/j.jseaes.2015.03.046>.
- Wu WJ, Wen S, Tang CC, Yeh YL, Lai HP, Dinh VQ and Chen CH (2018) Seismogenic structures in the Ma River fault zone, Vietnam: Insights from focal mechanisms of microearthquakes and local stress states. *Bulletin of the Seismological Society of America* 108(6): Article 6. <https://doi.org/10.1785/0120180096>.
- Zhao JX, Irikura K, Zhang J, Fukushima Y, Somerville PG, Asano A, Ohno Y, Oouchi T, Takahashi T and Ogawa H (2006) An empirical site-classification method for strong-motion stations in Japan using H/V response spectral ratio. *Bulletin of the Seismological Society of America* 96(3): 914–925. <https://doi.org/10.1785/0120050124>.